International Journal of Solids and Structures 49 (2012) 1–17

Contents lists available at SciVerse ScienceDirect

International Journal of Solids and Structures

journal homepage: www.elsevier.com/locate/ijsolstr

The effect of particle shape and distribution on the macroscopic behavior of magnetoelastic composites

Evan Galipeau [a], Pedro Ponte Castañeda [a,b,*]

[a] Department of Mechanical Engineering and Applied Mechanics, Graduate Group in Applied Mathematics and Computational Science, University of Pennsylvania, Philadelphia, PA 19104-6315, USA

[b] Madrid Institute for Advanced Studies of Materials (IMDEA-Materials), 28040 Madrid, Spain

ARTICLE INFO

Article history:
Received 2 June 2011
Received in revised form 26 August 2011
Available online 19 September 2011

Keywords:
Magnetoelasticity
Magnetostriction
Actuation pressure
Non-linear
Particulate media
Energy methods
Maxwell stress

ABSTRACT

The magnetoelastic homogenization framework and the partial decoupling approximation proposed by Ponte Castañeda and Galipeau (2011) are used to estimate material properties for a class of magnetically susceptible elastomers. Specifically, we consider composites consisting of aligned, ellipsoidal magnetic particles distributed randomly with "ellipsoidal" symmetry under combined magnetic and mechanical loading. The model captures the coupling between the magnetic and mechanical fields, including the effects of magnetic saturation. The results help elucidate the effects of particle shape, distribution, and concentration on properties such as the magnetostriction, actuation stress, magnetic modulus, and magnetization behavior of a magnetorheological composite.

1. Introduction

Magnetorheological elastomers (MREs) are composite materials exhibiting coupled magnetic and mechanical behavior. Typical MREs consist of magnetically susceptible particles embedded in a soft elastomer matrix. Frequently used magnetic materials include carbonyl iron and nickel; examples of more exotic inclusions are Terfenol-D and Ni_2MnGa. MREs are of interest because magnetic fields are capable of modifying the effective mechanical properties of the composite and of producing magnetostrictive strain. Both effects take place quickly and reversibly, making MREs good candidates for tunable vibration dampers and magnetic actuators.

Three primary mechanisms are responsible for the magneto-mechanical coupling in MREs: magnetostriction of the inclusions, magnetic torques on particles, and magnetic interactions between particles. For MREs containing particles of giant magnetostrictive materials, such as Terfenol-D and Ni_2MnGa, all three mechanisms can be important (Duenas and Carman, 2000). For other inclusion materials, such as carbonyl iron, nickel, or cobalt, which have very small magnetostriction, the particles are effectively rigid, and the principal mechanisms are magnetic torques and magnetic interactions between particles (Jolly et al., 1996; Bednarek, 1999; Ginder et al., 2002; Guan et al., 2008).

Experiments have been performed on MREs composed of rigid, magnetic particles by various researchers. The particles can either be distributed randomly in the composite or aligned in chain structures by curing the elastomer under application of a magnetic field. Jolly et al. (1996) performed shear tests on chain-structured MREs and showed that the magnetic field increases the effective shear modulus of the composite. Bednarek (1999) measured the magnetostriction of composites made with randomly distributed particles subjected to very high magnetic fields. Ginder et al. (2002) and Guan et al. (2008) determined experimentally the magnetostriction of random and chain structured MREs. Lanotte et al. (2003) investigated the effect of particle rotation on the average magnetization of the composite. More recently, Diguet et al. (2010) have provided experimental and theoretical results for the magnetostriction and magnetic saturation of composite samples formed into a cylindrical shape and exposed to a remotely applied magnetic field.

For MREs made from particles with small magnetostriction, Borcea and Bruno (2001) developed a theoretical model for composites composed of rigid, isotropic, ferromagnetic spheres by considering particle–particle forces, and obtained estimates that are accurate to second order in the volume fraction. To first order in the volume fraction, their results agree with the dilute limit of a rigidly reinforced composite because the inter-particle forces vanish in this limit, and, in addition, the isotropic spheres cannot experience magnetic torques. Yin and Sun (2006) also considered

* Corresponding author at: Department of Mechanical Engineering and Applied Mechanics, Graduate Group in Applied Mathematics and Computational Science, University of Pennsylvania, Philadelphia, PA 19104-6315, USA.

E-mail addresses: galipeau@seas.upenn.edu (E. Galipeau), ponte@seas.upenn.edu (P. Ponte Castañeda).

0020-7683/$ - see front matter © 2011 Elsevier Ltd. All rights reserved.
doi:10.1016/j.ijsolstr.2011.08.014

composites with randomly distributed isotropic spheres; however, the particles could deform elastically, but were assumed to exhibit linear magnetic behavior. In this work, the pairwise particle interactions were also used to compute an average stress over the composite, and to obtain magnetoelastic constitutive relations. Yin et al. (2006) extended this approach to MREs where the magnetic particles form chain structures, but still preserve their spherical shape.

On the other hand, Duenas and Carman (2000) obtained experimental results for MREs made with Terfenol-D inclusions at concentrations ranging from 10% to 50%, and estimated the concentration maximizing the composite magnetostriction. Liu et al. (2006) obtained estimates for the effective properties of MREs composed of giant magnetostrictive particles in the limit when the concentration of the particles is dilute, and for cases when the magnetic field is aligned with the symmetry axis of the particles. This work made use of a sophisticated theory to model the effect of particle magnetostriction, and showed the importance of this effect, but did not account for inter-particle forces, which vanish in the dilute limit, nor for particle torques, which were zero because of the symmetry of the loading.

More recently, Ponte Castañeda and Galipeau (2011) developed a general homogenization framework which is capable of determining the magnetoelastic properties of composite materials at finite strain. This general framework can in principle account for magnetostriction of the particles, particle rotations and inter-particle forces. However, when the particles can be assumed to be rigid, the underlying analysis can be simplified via a partial decoupling approximation (Ponte Castañeda and Galipeau, 2011) to obtain explicit estimates for the fully coupled magnetoelastic constitutive relations of the composite elastomer under general loading conditions. One advantage of this work is that it allows for more general particle shapes and distributions, as well as non-linear magnetic particle behavior, including the effect of magnetic saturation. In addition, this homogenization framework provides a simple estimate for the effective free-energy of the composite, from which the homogenized constitutive relations for the composite can be readily obtained. In contrast with the works of Borcea and Bruno (2001) and Yin and Sun (2006), this formulation obviates the need for the direct computation of the inter-particle forces in the composite, which is difficult to accomplish in practice. In this paper, the homogenization framework of Ponte Castañeda and Galipeau (2011) will be used to estimate the response of MREs containing aligned, spheroidal particles, distributed randomly in the elastic matrix with "spheroidal" symmetry (Willis, 1977).

The paper is organized as follows. Section 2 introduces some background material on finite-strain magnetoelasticity and gives a brief description of how to relate the total magnetoelastic stress to the actual traction measured in experiments. Section 3 begins with a summary of the magnetoelastic homogenization and partial decoupling approximation. In Section 3.1, the model is applied to composites with "ellipsoidal" microstructures subjected to aligned loading conditions. In Section 3.2 the results are specialized for small strains, and in Section 3.3 expressions are given for the surface traction in composite materials consisting of spheroidal particles with nonlinear magnetic behavior, distributed spheroidally in an isotropic non-magnetic matrix, and subjected to aligned loadings. Then, in Section 4 the results of the previous section are specialized for uniaxial loading aligned with the symmetry axis of the spheroidal inclusions. Finally, in Section 5, we investigate in some detail the effects of particle shape and concentration on the magnetoelastic behavior of the composite in the uniaxial tension test. The paper ends in Section 6 with some concluding remarks.

In this article, scalars will be denoted by italic Roman, a and G, or Greek letters, α; vectors by boldface Roman letters, $\mathbf{b}$; second-order tensors by boldface italic Roman letters, $\boldsymbol{P}$, or bold face Greek letters, $\boldsymbol{\epsilon}$; and fourth-order by tensors barred letters, $\mathbb{C}$. When necessary Cartesian components will be introduced; for example, C_{ijkl} are the Cartesian components of $\mathbb{C}$.

2. Magneto-elastostatics

In this work, we will consider the deformation of a heterogeneous material occupying a region Ω_0 in the reference configuration. Let each material point be defined by its position vector $\mathbf{X}$ in Ω_0. Under the combined action of the mechanical and magnetic effects, the material deforms to a new position described by $\mathbf{x}$ in the deformed configuration of the specimen Ω. The local deformation is characterized by the deformation gradient tensor $\boldsymbol{F} = \text{Grad}\,\mathbf{x}$, with Cartesian components $F_{ij} = \frac{\partial x_i}{\partial X_j}$, and such that $J = \det \boldsymbol{F} > 0$. The material satisfies the conservation of mass, which in local form becomes $\rho_0 = \rho J$, where ρ_0 and ρ are the material densities in the reference and deformed configurations, respectively. We also recall, for later use, that the polar decomposition of the deformation gradient is $\boldsymbol{F} = \boldsymbol{RU}$, where $\boldsymbol{R}$ is the rotation and $\boldsymbol{U}$ is the stretch tensor.

We define $\boldsymbol{T}$ to be the *total* Cauchy stress, which, at static equilibrium and in the absence of mechanical body forces, satisfies the governing equation:

$$\text{div}\,\boldsymbol{T} = 0, \tag{1}$$

as well as the symmetry condition $\boldsymbol{T}^{\mathrm{T}} = \boldsymbol{T}$. In this expression, div is the divergence operator with respect to $\mathbf{x}$. Note that this equation must be replaced by the continuity condition $[[\boldsymbol{T}]]\mathbf{n} = 0$ at an interface, where $\mathbf{n}$ is the normal to the interface.

In the current configuration, there are two primary magnetic field vectors: the magnetic intensity $\mathbf{h}$ and the magnetic induction $\mathbf{b}$. In the absence of surface and free currents, and for quasi-static conditions, they satisfy the conservation equations:

$$\text{div}\,\mathbf{b} = 0, \quad \text{and} \quad \text{curl}\,\mathbf{h} = 0, \tag{2}$$

where the div and curl operators are with respect to $\mathbf{x}$. The corresponding continuity conditions at an interface are given by $[[\mathbf{b}]] \cdot \mathbf{n} = 0$ and $[[\mathbf{h}]] \times \mathbf{n} = 0$, respectively.

The relation between these two fields is customarily defined in terms of the magnetization $\mathbf{m}$, such that:

$$\mathbf{h} = \frac{\mathbf{b}}{\mu_0} - \mathbf{m}, \tag{3}$$

where μ_0 is the magnetic permeability of vacuum. In Eq. (3), the magnetization is a field determined by the material occupying a given space, and it is a function of the magnetic field and the deformation (Kovetz, 2000).

Assuming the existence of a free-energy function $\phi(\boldsymbol{F},\mathbf{b})$, a thermodynamically consistent framework was developed by Kovetz (2000) by means of the method of Coleman and Noll (1963). In this framework, for quasi-static processes, the magnetic constitutive relation reduces to:

$$\mathbf{m} = -\rho \frac{\partial \phi}{\partial \mathbf{b}}, \tag{4}$$

while the total Cauchy stress is given by

$$\boldsymbol{T} = \rho \frac{\partial \phi}{\partial \boldsymbol{F}} \boldsymbol{F}^T - \frac{1}{2\mu_0}(\mathbf{b}\cdot\mathbf{b})\boldsymbol{I} + \frac{1}{\mu_0}\mathbf{b}\otimes\mathbf{b} + (\mathbf{m}\cdot\mathbf{b})\boldsymbol{I} - \mathbf{m}\otimes\mathbf{b}. \tag{5}$$

It follows that the energy function ϕ fully characterizes the behavior of the magnetoelastic materials. Note that in the absence of a material, or when the material is non-magnetic, there is still a stress which depends on the magnetic field, called the Maxwell stress. Also, note that the objectivity of ϕ implies the symmetry of $\boldsymbol{T}$, as required by rotational equilibrium.

In order to make comparisons with actual experiments, the relation between the applied traction and the total stress within the material must be determined. In elasticity, the applied traction is the normal component of the total stress at a surface, because the vacuum immediately surrounding the material contains no stress. In magnetoelasticity, the magnetic fields extend past the sample being tested and into the vacuum (or non-magnetic material) immediately outside. The magnetic field generates a Maxwell stress outside, which affects the mechanical traction measured. When a non-magnetic material is being tested, the magnetic stresses are self-equilibrated and magnetic fields have no effect on the traction. However, when the material is magnetic, the magnetic stresses are not equilibrated and contribute to the measurable traction on the boundary of the specimen. Based on the jump condition for the total Cauchy stress, $[[\boldsymbol{T}]]\mathbf{n} = 0$, and the magnetic jump conditions, $[[\mathbf{b}]] \cdot \mathbf{n} = 0$ and $[[\mathbf{h}]] \times \mathbf{n} = 0$, the magnetic field and subsequently the magnetic stress outside the material can be determined based on the magnetic fields inside the material, and it can be shown (Kankanala and Triantafyllidis, 2004) that the traction on the boundary of the specimen is given by

$$\mathbf{t} = \left[\boldsymbol{T} + \left(\frac{\mu_0}{2}(\mathbf{h}\cdot\mathbf{h})\boldsymbol{I} - \mathbf{h}\otimes\mathbf{b}\right)\right]\mathbf{n} - \frac{\mu_0}{2}(\mathbf{m}\cdot\mathbf{n})^2\mathbf{n}, \tag{6}$$

where $\boldsymbol{T}$, $\mathbf{h}$, $\mathbf{b}$, and $\mathbf{m}$ are the fields (in the material) just inside the boundary, and $\mathbf{n}$ is the outward normal to the boundary. It should also be emphasized that although this formula is easiest to write in terms of $\boldsymbol{T}$, $\mathbf{h}$, $\mathbf{b}$ and $\mathbf{m}$, these are not all independent variables. For instance if we specify $\mathbf{b}$ and $\boldsymbol{F}$, all other variables are determined by the magnetic and mechanical constitutive relations of the material. In addition, note that in the absence of a magnetic field, the above expression reduces to its usual form in the purely mechanical case, $\mathbf{t} = \boldsymbol{T}\mathbf{n}$.

3. Homogenization estimate for constitutive behavior of MREs

Constituent energy functions. We are interested in two-phase composites consisting of rigid particles in an elastomeric matrix. The approximation of rigid particles is quite accurate for MREs, since the modulus of the particles is several orders of magnitude higher than that of the soft elastomeric matrix. The energy for the non-magnetic matrix is given by functions of the form:

$$\phi^{\mathrm{mat}}(\boldsymbol{F},\mathbf{b}) = \frac{1}{\rho_0}W^{\mathrm{mat}}(\boldsymbol{F}), \tag{7}$$

where $W^{\mathrm{mat}}(\boldsymbol{F})$ is the stored-energy function for the elastomer in the absence of a magnetic field.

We also need an energy function to characterize the magnetic particles. In the limit of rigid behavior, the particles can be described by a function of the form:

$$\phi^{\mathrm{part}}(\boldsymbol{F},\mathbf{b}) = \frac{1}{\rho_0}W^{\mathrm{rig}}(\boldsymbol{F}) + \phi^{\mathrm{mag}}(\mathbf{b}). \tag{8}$$

The rigidity condition is enforced by $W^{\mathrm{rig}}(\boldsymbol{F})$, a mechanical energy function that is equal to zero if $\boldsymbol{F}$ is a pure rotation and infinity otherwise, while $\phi^{\mathrm{mag}}(\mathbf{b})$ is a function characterizing the magnetization of the inclusion in the current configuration. In this paper, we take the particles to be magnetically isotropic, but nonlinear, and we use a Langevin function as a phenomenological model to describe the magnetic behavior of the inclusion material. As discussed in Ponte Castañeda and Galipeau (2011), magnetic anisotropy is important for smaller particles, which can be single crystals, and this effect can be accounted for, provided that a good model is available for the anisotropic behavior for the single particles. Here, for simplicity, we assume isotropic behavior. Although other models could be used, the Langevin model should be adequate to describe approximately the behavior of particles made of materials, such as magnetically soft iron. The isotropic Langevin model accounts for the initial (linear) susceptibility χ and saturation magnetization m_s of the particle, so that the magnetic energy is a function of $b = |\mathbf{b}|$ given by

$$\rho_0\phi^{\mathrm{mag}}(\mathbf{b}) = -\frac{\mu_0 m_s^2}{3\chi}\left[\ln\left(\sinh\left[\frac{3\chi b}{\mu_0 m_s}\right]\right) - \ln\left(\frac{3\chi b}{\mu_0 m_s}\right)\right], \tag{9}$$

while the corresponding magnetization is given by

$$\mathbf{m}(\mathbf{b}) = \frac{m_s}{b}\left[\coth\left(\frac{3\chi b}{\mu_0 m_s}\right) - \frac{\mu_0 m_s}{3\chi b}\right]\mathbf{b}. \tag{10}$$

Composite energy function. Homogenization can be used to determine an effective energy for the composite material $\tilde{\phi}$ as a function of the average fields over the composite $\bar{\boldsymbol{F}}$ and $\bar{\mathbf{b}}$. Then, under the *separation of length scales* hypothesis, the composite can be treated as a homogenous material with a constitutive relation derived from $\tilde{\phi}$ using expressions (4) to (5). Also, the governing Eqs. (1)–(3) can be used to determine the macroscopic stress $\bar{\boldsymbol{T}}$, the magnetization $\bar{\mathbf{m}}$, and magnetic intensity $\bar{\mathbf{h}}$ in the specimen.

The partial decoupling approximation of Ponte Castañeda and Galipeau (2011) uses the special properties of the composites with particulate microstructures whose constituent energy functions are of form (7) and (8) to provide an expression for $\tilde{\phi}$. The partial decoupling approximation exploits the fact that the magnetic energy of the composite depends only on the position and orientation of the particles in the deformed configuration (and not on the local deformation of the matrix). As a result, the magnetoelastic energy can be approximated as the sum of a "purely mechanical" and a magnetoelastic contribution to the energy.

Thus, the effective free-energy function for the composite is of the form:

$$\tilde{\phi}(\bar{\boldsymbol{F}},\bar{\mathbf{b}}) = \frac{\widetilde{W}^{\mathrm{me}}(\bar{\boldsymbol{F}})}{\bar{\rho}_0} + \tilde{\phi}^{\mathrm{mag}}(\bar{\boldsymbol{F}},\bar{\mathbf{b}}), \tag{11}$$

where $\widetilde{W}^{\mathrm{me}}(\bar{\boldsymbol{F}})$ is the usual effective stored-energy function arising from the solution to the purely mechanical homogenization problem, and $\tilde{\phi}^{\mathrm{mag}}(\bar{\boldsymbol{F}},\bar{\mathbf{b}})$ is the effective free-energy function from the solution to the magnetostatic homogenization problem in the deformed configuration. This second term (or more precisely its derivative) can be interpreted physically as the deformation-dependent, magnetic susceptibility of the composite material. The coupling is achieved because $\tilde{\phi}^{\mathrm{mag}}(\bar{\boldsymbol{F}},\bar{\mathbf{b}})$ depends on $\bar{\boldsymbol{F}}$; in other words, $\tilde{\phi}^{\mathrm{mag}}(\bar{\boldsymbol{F}},\bar{\mathbf{b}})$ depends on the macroscopic deformation. As we will see in the following section, this produces contributions to the stress depending on the evolution of the microstructure induced by the deformation.

3.1. Aligned loading: constitutive response

In this section, we will specialize the general results of Ponte Castañeda and Galipeau (2011) for situations when the magnetic and mechanical loadings are aligned with the microstructure of the MRE. It is recalled from that work that the MREs are modeled as elastic materials containing random distributions of aligned particles. The particles are taken to have ellipsoidal shape and to be distributed randomly with "ellipsoidal" symmetry (Willis, 1977). Particulate microstructures of this type can be visualized, as shown in Fig. 1, as having ellipsoidal particles with principal lengths w_i^{l} surrounded by a distributional ellipsoid with principal lengths w_i^{D}. The distributional ellipsoid characterizes – through the two-point probability function of the microstructure – the average distance between the particles in different directions. The principal axes of both ellipsoids are assumed to be aligned, so that we can use the same set of unit vectors, $\hat{\mathbf{e}}_i$, to define the orientation of both

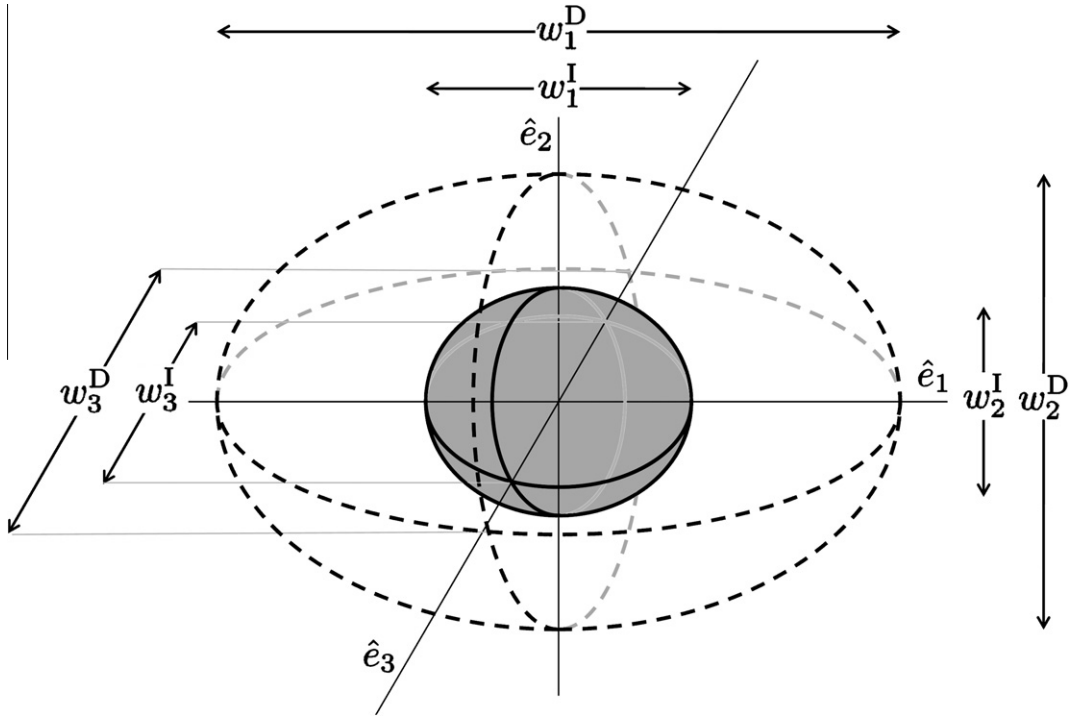

Fig. 1. A general ellipsoidal inclusion surrounded by its distributional ellipsoid. The principal axes of both ellipses are aligned with the coordinate system and have lengths w_i^{I} and w_i^{D}, respectively.

ellipsoids. We can then write the shape tensors $\boldsymbol{Z}^{\mathrm{I}}$ and $\boldsymbol{Z}^{\mathrm{D}}$, defining the shape and initial distribution of the inclusions, in the forms:

$$\boldsymbol{Z}^{\mathrm{I}} = \sum_{i=1}^{3} w_i^{\mathrm{I}} \hat{\mathbf{e}}_i \otimes \hat{\mathbf{e}}_i, \quad \text{and} \quad \boldsymbol{Z}^{\mathrm{D}} = \sum_{i=1}^{3} w_i^{\mathrm{D}} \hat{\mathbf{e}}_i \otimes \hat{\mathbf{e}}_i. \tag{12}$$

Under the above microstructural hypotheses, the MRE exhibits orthotropic symmetry and is such that no rotations will be induced in the microstructure if the magnetic and mechanical fields are aligned with the symmetry axes defined by the vectors $\hat{\mathbf{e}}_i$. Thus, the composite is assumed to be loaded magnetically along the kth direction, so that:

$$\bar{\mathbf{b}} = \bar{b}\hat{\mathbf{e}}_k, \tag{13}$$

where $\bar{b}$ is the magnitude of the magnetic flux. The deformation is also aligned (co-axial) with the symmetry axes, so the deformation gradient is described by

$$\overline{\boldsymbol{F}} = \overline{\boldsymbol{U}} = \sum_{i=1}^{3} \bar{\lambda}_i \hat{\mathbf{e}}_i \otimes \hat{\mathbf{e}}_i, \tag{14}$$

where $\bar{\lambda}_i$ is the (principal) stretch in the $\hat{\mathbf{e}}_i$ direction.

Under these conditions, the average magnetization in the MRE is given by

$$\bar{\mathbf{m}}(\bar{\mathbf{b}}) = \frac{1}{\mu_0} \widetilde{\boldsymbol{X}}_L(\overline{\boldsymbol{U}}, \chi_L)\bar{\mathbf{b}}, \tag{15}$$

where $\widetilde{\boldsymbol{X}}_L(\overline{\boldsymbol{U}}, \bar{\mathbf{b}})$ is the effective magnetic susceptibility of a linear comparison composite (see Ponte Castañeda, 1992, 1998) with linear magnetic susceptibility χ_L in the matrix phase. Using the linear homogenization procedure of Ponte Castañeda and Willis (1995) for the above-defined microstructure, the following expression is obtained:

$$\widetilde{\boldsymbol{X}}_L(\overline{\boldsymbol{U}}, \chi_L) = \frac{c^{\mathrm{I}}}{\bar{J}} \left[\frac{\boldsymbol{I}}{\chi_L} - \boldsymbol{I} + \boldsymbol{P}^{\mathrm{I}} + \frac{c^{\mathrm{I}}}{\bar{J}} \boldsymbol{I} - c^{\mathrm{I}} \boldsymbol{P}^{\mathrm{D}}(\overline{\boldsymbol{U}}) \right]^{-1}, \tag{16}$$

where c^{I} is the concentration of inclusions, and $\boldsymbol{P}^{\mathrm{I}}$ and $\boldsymbol{P}^{\mathrm{D}}$ are microstructural tensors, characterizing the effects of the inclusions and distribution, and given by

$$\boldsymbol{P}^{\mathrm{I}} = \frac{\det \boldsymbol{Z}^{\mathrm{I}}}{4\pi} \int_{|\xi|=1} \xi \otimes \xi \; | \, \boldsymbol{Z}^{\mathrm{I}} \xi |^{-3} dS(\xi), \tag{17}$$

and

$$\boldsymbol{P}^{\mathrm{D}}(\overline{\boldsymbol{U}}) = \frac{\det \boldsymbol{Z}^{\mathrm{D}}}{4\pi} \int_{|\xi|=1} \xi \otimes \xi \left| \boldsymbol{Z}^{\mathrm{D}} \overline{\boldsymbol{U}} \xi \right|^{-3} dS(\xi). \tag{18}$$

In addition, the comparison susceptibility χ_L is determined from the solution of the "secant" linearization equation (Ponte Castañeda, 1998):

$$\frac{1}{\mu_0 c^{\mathrm{I}}} \widetilde{\boldsymbol{X}}_L(\overline{\boldsymbol{U}}, \chi_L)\bar{\mathbf{b}} = \mathbf{m}\left(\mathbf{b} = \frac{\widetilde{\boldsymbol{X}}_L(\overline{\boldsymbol{U}}, \chi_L)\bar{\mathbf{b}}}{c^{\mathrm{I}} \chi_L} \right), \tag{19}$$

where $\mathbf{m}$ is given as a function of $\mathbf{b}$ by expression (10). Even though this equation is a vector equation, $\mathbf{m}(\mathbf{b})$ is such that both sides of the equation are parallel, producing only one independent equation to determine χ_L. Also it may appear in Eq. (15) that the magnetization $\bar{\mathbf{m}}$ is linear in the applied magnetic field; however χ_L depends on $\bar{\mathbf{b}}$ so the magnetization is nonlinear in the magnetic flux and also depends on the deformation through $\bar{J}$ and $\boldsymbol{P}^{\mathrm{D}}(\overline{\boldsymbol{U}})$.

Correspondingly, the total Cauchy stress is given by

$$\begin{aligned} \overline{\boldsymbol{T}} = \overline{\boldsymbol{T}}^{\mathrm{me}}(\overline{\boldsymbol{U}}) &- \frac{1}{2\mu_0}(\bar{\mathbf{b}} \cdot \bar{\mathbf{b}})\boldsymbol{I} + \frac{1}{\mu_0} \bar{\mathbf{b}} \otimes \bar{\mathbf{b}} + (\bar{\mathbf{m}} \cdot \bar{\mathbf{b}})\boldsymbol{I} - \bar{\mathbf{m}} \otimes \bar{\mathbf{b}} \\ &- \frac{\mu_0}{2}(\bar{\mathbf{m}} \cdot \bar{\mathbf{m}})\boldsymbol{I} - \frac{\mu_0}{2} \bar{J} \frac{\partial}{\partial \overline{\boldsymbol{U}}} \left[\bar{\mathbf{m}} \cdot \boldsymbol{P}^{\mathrm{D}}(\overline{\boldsymbol{U}}) \bar{\mathbf{m}} \right] \overline{\boldsymbol{U}}, \end{aligned} \tag{20}$$

where

$$\overline{\boldsymbol{T}}^{\rm me}(\overline{\boldsymbol{F}}) = \frac{\rho}{\rho_0}\frac{\partial \widetilde{W}^{\rm me}(\overline{\boldsymbol{F}})}{\partial \overline{\boldsymbol{F}}}\overline{\boldsymbol{F}}^{\rm T}, \tag{21}$$

is the purely mechanical stress, and $\bar{\mathbf{m}}$ is given in terms of $\overline{\boldsymbol{U}}$ and $\bar{\mathbf{b}}$ via expression (15). Note, however, that the derivatives with respect to $\overline{\boldsymbol{U}}$ in Eq. (20) are taken with $\bar{\mathbf{m}}$ held fixed.

By comparing expression (20) for the homogenized stress with expression (5) for the stress in a general magnetoelastic material, it can be seen that, in addition to the usual magnetic terms, and to the purely mechanical stress, there are two additional terms arising from the derivatives of the effective free-energy with respect to the deformation that are quadratic in the magnetization. The first is a hydrostatic pressure which can be directly related to changes in the concentration of the particles with the deformation, while the second involves changes in the shape of the two-point distribution of the particles with the deformation. They both come from the second term in expression (11) for the effective energy function, which describes the nonlinear magnetic susceptibility of the composite. In this context, it is interesting to remark that while the particle–particle forces have *not* been computed directly, the estimate (20) for the macroscopic stress does include these two-point interactions between the particles, as has just been remarked. In fact, this new method for determining the macroscopic stress of the MRE requires only the computation of derivatives of the nonlinear magnetic susceptibility of the composite. As a consequence, it is simpler to implement and generalize than other methods requiring the direct computation of the particle–particle forces (Borcea and Bruno, 2001; Yin and Sun, 2006), which is much more involved in practice.

Since the loading is aligned with the principal axes, which are symmetry axes for the composite, the second-order tensors $\overline{\boldsymbol{T}}$, $\widetilde{\boldsymbol{X}}_L$, $\boldsymbol{P}^{\rm I}$ and $\boldsymbol{P}^{\rm D}$ can be written in terms of their principal values as:

$$\begin{aligned}&\overline{\boldsymbol{T}} = \sum_{i=1}^{3}\overline{T}_i\hat{\mathbf{e}}_i\otimes\hat{\mathbf{e}}_i, \quad \widetilde{\boldsymbol{X}}_L = \sum_{i=1}^{3}\widetilde{X}_{L_i}\hat{\mathbf{e}}_i\otimes\hat{\mathbf{e}}_i,\\ &\boldsymbol{P}^{\rm I} = \sum_{i=1}^{3}P_i^{\rm I}\hat{\mathbf{e}}_i\otimes\hat{\mathbf{e}}_i, \quad \text{and} \quad \boldsymbol{P}^{\rm D} = \sum_{i=1}^{3}P_i^{\rm D}\hat{\mathbf{e}}_i\otimes\hat{\mathbf{e}}_i.\end{aligned} \tag{22}$$

Therefore, the magnetization is aligned with the **b** field, as given by expression (13), so that $\bar{\mathbf{m}} = \bar{m}\hat{\mathbf{e}}_k$ with:

$$\bar{m} = \widetilde{X}_{L_k}\bar{b} = \frac{c^{\rm I}\chi_L\bar{b}}{1-\chi_L\left[1-P_k^{\rm I}+c^{\rm I}\left(P_k^{\rm D}-1\right)\right]}, \tag{23}$$

where it is recalled that the $P_k^{\rm D}$ are functions of the principal stretches $\bar{\lambda}_i$. Thus, expression (23) provides the average magnetization in the MRE resulting from the application of a **b** field in the k-direction, as a function of $\bar{b}$ and the $\bar{\lambda}_i$, for a given volume fraction of the particles and particle and distribution shapes.

Corresponding expressions can be also obtained from expression (20) for the principal components $\overline{T}_i$ of the average stress, as functions of $\bar{b}$ and the $\bar{\lambda}_i$. However, as we have already seen in the context of expression (6), the actual tractions $\bar{t}_i$ that would need to be applied on the boundaries of a representative volume element of the MRE would be different from the principal stresses $\overline{T}_i$, and would depend on the boundary normals. Assuming that the boundaries of the specimen are perpendicular to the symmetry directions, such that $\mathbf{n}_i = \hat{\mathbf{e}}_i$, expression (6) gives the following results in each of the 3 symmetry directions:

$$\bar{t}_i = \overline{T}_i - \frac{\bar{b}^2}{2\mu_0} \quad \text{for} \quad i=k, \quad \text{and} \quad \bar{t}_i = \overline{T}_i + \frac{\mu_0\bar{h}^2}{2} \quad \text{for} \quad i\neq k, \tag{24}$$

where it is recalled that k is a fixed number denoting the magnetic field direction, and that $\bar{h}$ is defined by $\bar{\mathbf{h}} = \bar{h}\hat{\mathbf{e}}_k$. Then, making use of Eq. (20) for the total stress components, the following magnetoelastic traction-stretch relations are obtained:

$$\bar{t}_i = \overline{T}_i^{\rm me}(\bar{\lambda}_i) - \frac{\mu_0}{2}\bar{m}^2\delta_{ik} - \frac{\mu_0}{2}\bar{J}\bar{m}^2\frac{\partial P_k^{\rm D}}{\partial\bar{\lambda}_i}\bar{\lambda}_i \quad \text{no sum}, \quad i=1,\ldots,3, \tag{25}$$

where $\overline{T}_i^{\rm me}$ is the principal component of the purely mechanical stress tensor (21), and δ_{ij} is the Kronecker delta (meaning that the second term only contributes when i is in the direction of the applied field k).

It is evident from expression (25) that the traction depends on the magnetic field only through the magnetization (i.e., $\bar{m}^2$), even though the total stress, as given by (20), includes terms that are proportional to $\bar{b}^2$ and $\bar{b}\bar{m}$. This means that while the total stress continues to rise in the MRE as the magnetic field is increased, the traction will necessarily saturate with magnetization, which is consistent with experimental observation for actual MREs (Bednarek, 1999; Ginder et al., 2002; Guan et al., 2008). In addition, noting that the average magnetization is linear in the particle concentration to leading order, it is easily deduced that the magnetic part of the traction, again to leading order, is of second order in the concentration, even though the total Cauchy stress includes terms that are of first order in the concentration. This result means that the first-order contributions to the total stress must cancel exactly with the magnetic stresses that are set up by the MRE just outside the specimen. This result is physically consistent, since at low concentrations, each particle behaves like an isolated particle in a uniform magnetic field and experiences no net magnetic force and therefore does not contribute to the traction. This result is also consistent with experimental results, as we shall see below.

3.2. Small-strain approximation

The traction-stretch relations (25) are valid for large strains, and arbitrary magnetic fields. In this work, however, we are interested in the limit of small strains (but still arbitrary magnetic fields), when the general expressions (23) and (25) for the average magnetization and traction, as functions of the stretch and magnetic field, simplify. The infinitesimal strain tensor $\bar{\boldsymbol{\epsilon}}$ is aligned with the stretch tensor $\overline{\boldsymbol{U}}$, as given by (14), so that:

$$\bar{\boldsymbol{\epsilon}} = \sum_{i=1}^{3}\bar{\epsilon}_i\hat{\mathbf{e}}_i\otimes\hat{\mathbf{e}}_i, \tag{26}$$

where $\bar{\epsilon}_i = \bar{\lambda}_i - 1$ and $|\bar{\epsilon}_i| \ll 1$. It then follows that the magnetization can be expanded for small strains, and Eq. (23) can be written as:

$$\bar{m} = \bar{m}^{(0)}(\bar{b}) + \sum_{i=1}^{3}\bar{m}_i^{(1)}(\bar{b})\bar{\epsilon}_i + o(\bar{\epsilon}^2), \tag{27}$$

where

$$\bar{m}^{(0)}(\bar{b}) = \bar{m}\big|_{\bar{\lambda}_1=\bar{\lambda}_2=\bar{\lambda}_3=1} \quad \text{and} \quad \bar{m}_i^{(1)}(\bar{b}) = \left.\frac{\partial\bar{m}}{\partial\bar{\lambda}_i}\right|_{\bar{\lambda}_1=\bar{\lambda}_2=\bar{\lambda}_3=1}. \tag{28}$$

In these expressions, and in the expressions to follow, the vertical bars mean with their arguments (in this case, $\bar{\lambda}_1, \bar{\lambda}_2, \bar{\lambda}_3$) held fixed (equal to 1).

The tractions can also be expanded for small strains, and under the aligned loading assumption, they reduce to expressions of the form:

$$\bar{t}_i = \bar{t}_i^{(0)}(\bar{b}) + \sum_{j=1}^{3}\widetilde{C}_{ij}^{\rm tot}(\bar{b})\bar{\epsilon}_j + o(\bar{\epsilon}^2), \tag{29}$$

where $\bar{t}_i^{(0)}$ denote the tractions at zero strain, also called the actuation stresses, and are functions of $\bar{b}$. They are given by

$$\bar{t}_i^{(0)} = -\frac{\mu_0}{2}\left(\bar{m}^{(0)}(\bar{b})\right)^2\left[\delta_{ik} + \left.\frac{\partial P_k^{\rm D}}{\partial\bar{\lambda}_i}\right|_{\bar{\lambda}_1=\bar{\lambda}_2=\bar{\lambda}_3=1}\right]. \tag{30}$$

On the other hand, $\widetilde{C}_{ij}^{\rm tot}(\bar{b})$ is a matrix representing the effective total modulus of the composite. It should be noted that the elements of $\widetilde{C}_{ij}^{\rm tot}$ are not the components of any general fourth-order elasticity tensor, but simply relate the axial tractions to the axial strains in this test. It should also be noted that $\widetilde{C}_{ij}^{\rm tot}(\bar{b})$ can be broken into a purely mechanical and a magnetic contribution, according to:

$$\widetilde{C}_{ij}^{\rm tot}(\bar{b}) = \widetilde{C}_{ij}^{\rm me} + \widetilde{C}_{ij}^{\rm mag}(\bar{b}). \tag{31}$$

The magnetic contribution of the modulus is given by

$$\widetilde{C}_{ij}^{\rm mag} = \frac{\mu_0\left(\bar{m}^{(0)}(\bar{b})\right)^2}{2}\left[-\left.\frac{\partial P_k^{\rm D}}{\partial\bar{\lambda}_i\partial\bar{\lambda}_j}\right|_{\bar{\lambda}_1=\bar{\lambda}_2=\bar{\lambda}_3=1} - (1+\delta_{ij})\left.\frac{\partial P_k^{\rm D}}{\partial\bar{\lambda}_i}\right|_{\bar{\lambda}_1=\bar{\lambda}_2=\bar{\lambda}_3=1}\right] + \mu_0\left(\bar{m}^{(0)}(\bar{b})\right)\left(\bar{m}_j^{(1)}(\bar{b})\right)\left[-\delta_{ik} - \left.\frac{\partial P_k^{\rm D}}{\partial\bar{\lambda}_i}\right|_{\bar{\lambda}_1=\bar{\lambda}_2=\bar{\lambda}_3=1}\right] \quad \text{(no sum)}, \tag{32}$$

while the purely mechanical component is extracted from the elasticity modulus $\tilde{\mathbb{C}}^{\rm me}$ of the MRE relating the mechanical stress $\overline{\boldsymbol{T}}^{\rm me}$ to the strain $\bar{\boldsymbol{\epsilon}}$ via:

$$\overline{\boldsymbol{T}}^{\rm me} = \tilde{\mathbb{C}}^{\rm me}\bar{\boldsymbol{\epsilon}}. \tag{33}$$

For rigid inclusions, the effective modulus of the composite can be given in terms of the matrix modulus $\mathbb{C}^{\rm mat}$, as:

$$\tilde{\mathbb{C}}^{\rm me} = \mathbb{C}^{\rm mat} + c^{\rm I}(\mathbb{P}^{\rm I} - c^{\rm I}\mathbb{P}^{\rm D})^{-1}. \tag{34}$$

where $\mathbb{P}^{\rm I}$ and $\mathbb{P}^{\rm D}$, are microstructural tensors, respectively describing the particle and distribution shapes (Ponte Castañeda and Willis, 1995). Note that $\widetilde{C}_{ij}^{\rm me} = \tilde{C}_{iijj}^{\rm me}$(no sum) for aligned loadings.

3.3. Spheroidal microstructure with incompressible matrix

The previous results apply for general ellipsoidal shapes for the particles and the distribution. However, in this section, we specialize these general results for the case where both the particles and the distribution exhibit a spheroidal shape with the same symmetry axes. Then, the MRE becomes transversely isotropic with the symmetry axis given by the axis of revolution of the particles, which we identify with $\hat{\mathbf{e}}_1$. In addition, we have that $w_2^{\rm I} = w_3^{\rm I} = w_2^{\rm D} = w_3^{\rm D} = 1$ with $w^{\rm D} = w_1^{\rm D}$ and $w^{\rm I} = w_1^{\rm I}$, and we can obtain explicit analytical expressions for the relevant microstructural tensors, and the corresponding expressions for the effective properties simplify considerably. Thus, the zero-strain average magnetization associated with the magnetic load (13) is obtained from expression (23), and given by

$$\bar{m}^{(0)}(\bar{b}) = \frac{c^{\rm I}\chi_L\bar{b}}{1-\chi_L(1-P_k(w^{\rm I})+c^{\rm I}[P_k(w^{\rm D})-1])}, \tag{35}$$

where

$$P_1(w) = \begin{cases} \dfrac{1}{1-w^2} - \dfrac{w\arccos(w)}{(1-w^2)^{3/2}} & w<1 \\ 1/3 & w=1 \\ \dfrac{1}{1-w^2} + \dfrac{w\ \mathrm{arccosh}(w)}{(-1+w^2)} & w>1 \end{cases}, \tag{36}$$

and

$$P_2(w) = P_3(w) = \begin{cases} \dfrac{w^2}{2(-1+w^2)} + \dfrac{w\arccos(w)}{2(1-w^2)^{3/2}} & w<1 \\ 1/3 & w=1 \\ \dfrac{w^2}{2(-1+w^2)} - \dfrac{w\ \mathrm{arccosh}(w)}{2(-1+w^2)^{3/2}} & w>1 \end{cases}. \tag{37}$$

Note that $w^{\rm D} \neq w^{\rm I}$, in general.

The corresponding expression for the linear comparison susceptibility χ_L, obtained from (19) specialized to the Langevin model, is given by

$$\frac{\bar{b}}{\mu_0 m_{\rm s}}\frac{\chi_L}{1-\chi_L\left[1-P_k^{\rm I}+c^{\rm I}\left(P_k^{\rm D}-1\right)\right]} = \coth\left(\frac{\bar{b}}{\mu_0 m_{\rm s}}\frac{3\chi}{\left(1-\chi_L\left[1-P_k^{\rm I}+c^{\rm I}\left(P_k^{\rm D}-1\right)\right]\right)}\right) - \frac{\mu_0 m_{\rm s}}{\bar{b}}\frac{\left(1-\chi_L\left[1-P_k^{\rm I}+c^{\rm I}\left(P_k^{\rm D}-1\right)\right]\right)}{3\chi}. \tag{38}$$

Explicit expressions for $\bar{t}_i^{(0)}$ can also be obtained for spheroidal microstructures from Eq. (30), together with the expressions in Appendix A for the derivatives of the $\boldsymbol{P}^{\rm D}$ with respect to $\boldsymbol{U}$. On the other hand, the expressions for $\bar{m}_i^{(1)}(\bar{b})$ and $\widetilde{C}_{ij}^{\rm mag}$ are more complicated and will not be given explicitly here. However, we will provide special forms for these quantities further below in the important limits of small and large magnetic fields.

In applications, it is important to consider incompressible matrix materials, leading to an indeterminate hydrostatic pressure p in the traction-strain relation (29) for the composite, such that:

$$\bar{t}_i = -p + \bar{t}_i^{(0)} + \sum_{j=1}^{3}\widetilde{C}_{ij}^{\rm tot}\bar{\epsilon}_j, \tag{39}$$

where the constraint that $\bar{\epsilon}_1+\bar{\epsilon}_2+\bar{\epsilon}_3=0$ must be enforced. In this case, the expressions for the elasticity moduli of the transversely isotropic composite simplify (Ponte Castañeda and Willis, 1995), and the components of $\tilde{\mathbb{C}}^{\rm me}$ can be expressed in terms of three different shear moduli, $\widetilde{G}_{\rm p}$, $\widetilde{G}_{\rm n}$ and $\widetilde{G}_{\rm a}$, corresponding to shear transverse to the fiber axis, longitudinal shear in the direction of the fiber axis and axisymmetric shear, respectively. They are given in terms of the shear modulus of the matrix G as:

$$\frac{\widetilde{G}_{\rm p}(w^{\rm I},w^{\rm D})}{G} = 1 + c^{\rm I}4\left[\frac{3h(w^{\rm I})-2(w^{\rm I})^2}{\left(1-(w^{\rm I})^2\right)} - c^{\rm I}\frac{3h(w^{\rm D})-2(w^{\rm D})^2}{\left(1-(w^{\rm D})^2\right)}\right]^{-1}, \tag{40}$$

$$\frac{\widetilde{G}_{\rm n}(w^{\rm I},w^{\rm D})}{G} = 1 + c^{\rm I}2\left[\frac{\left[\left(1+(w^{\rm I})^2\right)(2-3h(w^{\rm I}))\right]}{\left(1-(w^{\rm I})^2\right)} - c^{\rm I}\frac{\left[\left(1+(w^{\rm D})^2\right)(2-3h(w^{\rm D}))\right]}{\left(1-(w^{\rm D})^2\right)}\right]^{-1}, \tag{41}$$

$$\frac{\widetilde{G}_{\rm a}(w^{\rm I},w^{\rm D})}{G} = 1 + c^{\rm I}\frac{2}{3}\left[\frac{\left[h(w^{\rm I})-2(w^{\rm I})^2+2(w^{\rm I})^2h(w^{\rm I})\right]}{\left(1-(w^{\rm I})^2\right)} - c^{\rm I}\frac{\left[h(w^{\rm D})-2(w^{\rm D})^2+2(w^{\rm D})^2h(w^{\rm D})\right]}{\left(1-(w^{\rm D})^2\right)}\right]^{-1}, \tag{42}$$

with

$$h(w) = \begin{cases} \dfrac{w[\arccos(w)-w\sqrt{1-w^2}]}{(1-w^2)^{3/2}} & w<1 \\ 2/3 & w=1 \\ \dfrac{w\left[w\sqrt{w^2-1}-\arccos(w)\right]}{(w^2-1)^{3/2}} & w>1 \end{cases}. \tag{43}$$

In any case, under the aligned loading conditions assumed here, only the transverse and axisymmetric shear moduli are relevant, and they can be related to the components of $\widetilde{C}_{ij}^{\rm me}$ via:

$$\begin{bmatrix} \widetilde{C}_{11}^{\rm me} & \widetilde{C}_{12}^{\rm me} & \widetilde{C}_{13}^{\rm me} \\ \widetilde{C}_{21}^{\rm me} & \widetilde{C}_{22}^{\rm me} & \widetilde{C}_{23}^{\rm me} \\ \widetilde{C}_{31}^{\rm me} & \widetilde{C}_{32}^{\rm me} & \widetilde{C}_{33}^{\rm me} \end{bmatrix} = \begin{bmatrix} \frac{4}{3}\widetilde{G}_{\rm a} & -\frac{2}{3}\widetilde{G}_{\rm a} & -\frac{2}{3}\widetilde{G}_{\rm a} \\ -\frac{2}{3}\widetilde{G}_{\rm a} & \frac{1}{3}\widetilde{G}_{\rm a}+\widetilde{G}_{\rm p} & \frac{1}{3}\widetilde{G}_{\rm a}-\widetilde{G}_{\rm p} \\ -\frac{2}{3}\widetilde{G}_{\rm a} & \frac{1}{3}\widetilde{G}_{\rm a}-\widetilde{G}_{\rm p} & \frac{1}{3}\widetilde{G}_{\rm a}+\widetilde{G}_{\rm p} \end{bmatrix}. \tag{44}$$

4. Axisymmetric microstructure and loading: uniaxial tension test

The theory developed in the previous section for spheroidal inclusions and distributions is valid for $w^{\mathrm{D}} \neq w^{\mathrm{I}}$; however, in this section, for simplicity, it will be assumed that $w = w^{\mathrm{D}} = w^{\mathrm{I}}$. In addition, as depicted in Fig. 2, we let $\hat{\mathbf{e}}_1$ be the axis of symmetry for the inclusion and distributional spheroids, and assume that the magnetic field is aligned with this symmetry direction such that $\bar{\mathbf{b}} = \bar{b}\hat{\mathbf{e}}_1$. Similarly, we consider axial traction such that $\bar{t}_1 = \bar{t}$ with $\bar{t}_2 = \bar{t}_3 = 0$. Under these conditions, the isotropic symmetry in the transverse plane defined by $\hat{\mathbf{e}}_2$ and $\hat{\mathbf{e}}_3$, together with the incompressibility constraint imply that the system can be described by a single strain parameter $\bar{\epsilon} = \bar{\epsilon}_1 = -2\bar{\epsilon}_2 = -2\bar{\epsilon}_3$.

4.1. Magnetization response

In terms of $\bar{\epsilon}$, the magnetization can then be written as:

$$\bar{m} = \bar{m}^{(0)}(\bar{b}) + \left[\bar{m}_1^{(1)}(\bar{b}) - \frac{\bar{m}_2^{(1)}}{2}(\bar{b}) - \frac{\bar{m}_3^{(1)}}{2}(\bar{b})\right]\bar{\epsilon} = \bar{m}^{(0)}(\bar{b}) + \bar{m}^{(1)}(\bar{b})\bar{\epsilon}. \tag{45}$$

Because of the nonlinear magnetic behavior, the expressions for $\bar{m}^{(0)}$ and $\bar{m}^{(1)}$, as functions of $\bar{b}$, are complicated. However, simple expressions can be obtained by considering the limits of small and large $\bar{b}$, respectively, corresponding to linear and saturation magnetization responses.

Small $\bar{b}$ limit. For the case of small $\bar{b}$, the magnetization is proportional to the magnetic flux so that:

$$\mu_0\bar{m} = \tilde{\chi}_{\mathrm{i}}\bar{b}, \tag{46}$$

where $\tilde{\chi}_{\mathrm{i}}$ represents the initial susceptibility of the composite, which depends on the strain, but not on $\bar{b}$. It can thus be written as:

$$\tilde{\chi}_{\mathrm{i}} = \left.\frac{\partial\bar{m}}{\partial\bar{b}}\right|_{\bar{b}=0} = \tilde{\chi}_{\mathrm{i}}^{(0)} + \tilde{\chi}_{\mathrm{i}}^{(1)}\bar{\epsilon}, \tag{47}$$

where $\tilde{\chi}_{\mathrm{i}}^{(0)}$ is the initial susceptibility of the composite at zero strain given by

$$\tilde{\chi}_{\mathrm{i}}^{(0)} = \mu_0\left.\frac{\partial\bar{m}^{(0)}}{\partial\bar{b}}\right|_{\bar{b}=0} = \begin{cases} -\dfrac{c^{\mathrm{I}}\chi(1-w^2)^{3/2}}{\sqrt{1-w^2}(w^2[\chi(c^{\mathrm{I}}-1)+1]-1)-w\chi(c^{\mathrm{I}}-1)\arccos(w)} & w<1 \\ \dfrac{3c^{\mathrm{I}}\chi}{3+2(c^{\mathrm{I}}-1)\chi} & w=1 \\ \dfrac{c^{\mathrm{I}}\chi(-1+w^2)^{3/2}}{\sqrt{-1+w^2}(w^2[\chi(c^{\mathrm{I}}-1)+1]-1)-w\chi(c^{\mathrm{I}}-1)\operatorname{arccosh}(w)} & w>1 \end{cases}. \tag{48}$$

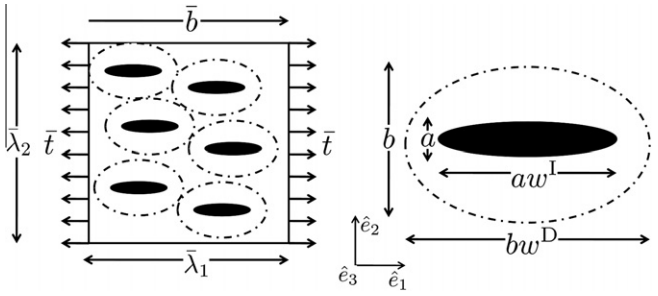

Fig. 2. Relevant loading conditions and material variables for composites with axial symmetry. The composite consists of spheroidal particles with aspect ratio w^{I} and distributional spheroid with aspect ratio w^{D}. The magnetic field and stretch are aligned with the particle aspect ratio and the normal traction on the surface.

and $\tilde{\chi}_{\mathrm{i}}^{(1)}$ is a correction accounting for the strain given by

$$\tilde{\chi}_{\mathrm{i}}^{(1)} = \mu_0\left.\frac{\partial\bar{m}^{(1)}}{\partial\bar{b}}\right|_{\bar{b}=0} = \begin{cases} \dfrac{3w(c^{\mathrm{I}})^2\chi^2\sqrt{1-w^2}[3w\sqrt{1-w^2}-(1+2w^2)\arccos(w)]}{2[\sqrt{1-w^2}(w^2[\chi(1-c^{\mathrm{I}})-1]+1)+w\chi(c^{\mathrm{I}}-1)\arccos(w)]^2} & w<1 \\ \dfrac{18(c^{\mathrm{I}})^2\chi^2}{5[3+2(c^{\mathrm{I}}-1)\chi]^2} & w=1 \\ \dfrac{3w(c^{\mathrm{I}})^2\chi^2\sqrt{-1+w^2}[3w\sqrt{-1+w^2}-(1+2w^2)\operatorname{arccosh}(w)]}{2[\sqrt{-1+w^2}(w^2[\chi(1-c^{\mathrm{I}})-1]+1)+w\chi(c^{\mathrm{I}}-1)\operatorname{arccosh}(w)]^2} & w>1 \end{cases}. \tag{49}$$

Large $\bar{b}$ limit. In the limit as $\bar{b}\to\infty$, the composite will reach magnetic saturation with magnetization given by

$$\bar{m}_{\mathrm{s}} = \lim_{\bar{b}\to\infty}\bar{m} = \bar{m}_{\mathrm{s}}^{(0)} + \bar{m}_{\mathrm{s}}^{(1)}\bar{\epsilon}, \tag{50}$$

where

$$\bar{m}_{\mathrm{s}}^{(0)} = \lim_{\bar{b}\to\infty}\bar{m}^{(0)} = c^{\mathrm{I}}m_{\mathrm{s}}, \tag{51}$$

and

$$\bar{m}_{\mathrm{s}}^{(1)} = \lim_{\bar{b}\to\infty}\bar{m}^{(1)} = 0. \tag{52}$$

These expressions can be easily derived by considering the composite saturation at finite strain. In the limit as $\bar{b}\to\infty$, all the particles saturate so the composite magnetization will be the product of the particle saturation magnetization and the current volume fraction. For an incompressible composite the particle concentration is fixed; therefore, $\bar{m}_{\mathrm{s}} = c^{\mathrm{I}}m_{\mathrm{s}}$, independently of the strain. This result is consistent with the recent experimental and theoretical predictions given by Diguet et al. (2010).

4.2. Mechanical response

Under uniaxial loading, the composite symmetry and incompressibility allow the reduction of Eq. (39) to the following expression for the uniaxial traction:

$$\bar{t} = \bar{t}^{(0)}(\bar{b}) + \widetilde{E}^{\mathrm{tot}}(\bar{b})\bar{\epsilon}. \tag{53}$$

In this expression, $\bar{t}^{(0)}$ corresponds to the traction at $\bar{\epsilon} = 0$. It is the effective uniaxial actuation stress of the composite, and is given by

$$\bar{t}^{(0)}(\bar{b}) = \mu_0\left(\bar{m}^{(0)}(\bar{b})\right)^2 D^{(0)}(w), \tag{54}$$

where $D^{(0)}(w)$ is a geometric factor defined by

$$D^{(0)}(w) = \left.\left(-1/2 - \frac{1}{2}\frac{\partial P_1^{\mathrm{D}}}{\partial\bar{\lambda}_1} + \frac{1}{2}\frac{\partial P_1^{\mathrm{D}}}{\partial\bar{\lambda}_2}\right)\right|_{\bar{\lambda}_1=\bar{\lambda}_2=\bar{\lambda}_3=1} = \begin{cases} -\dfrac{2+5w^2+2w^2}{4(-1+w^2)^2} + \dfrac{3w(1+2w^2)\arccos(w)}{4(1-w^2)^{5/2}} & w<1 \\ -3/10 & w=1 \\ -\dfrac{2+5w^2+2w^2}{4(-1+w^2)^2} + \dfrac{3w(1+2w^2)\operatorname{arccosh}(w)}{4(-1+w^2)^{5/2}} & w>1 \end{cases}. \tag{55}$$

On the other hand, $\widetilde{E}^{\mathrm{tot}}$ is the effective total Young's modulus for the composite, which can be broken up into a purely mechanical part and a part depending on $\bar{b}$, such that:

$$\widetilde{E}^{\mathrm{tot}}(\bar{b}) = \widetilde{E}^{\mathrm{me}} + \widetilde{E}^{\mathrm{mag}}(\bar{b}). \tag{56}$$

Thus, $\widetilde{E}^{\mathrm{me}}$ is the mechanical Young's modulus for the composite in the axial direction, such that $\widetilde{E}^{\mathrm{me}} = 3\widetilde{G}_{\mathrm{a}}$, where $\widetilde{G}_{\mathrm{a}}$ is given by Eq. (43). The magnetic modulus $\widetilde{E}^{\mathrm{mag}}$ depends on the applied magnetic field $\bar{b}$ in a complicated fashion; however, as was the case for

the magnetization, simpler expressions may be generated by considering the small and large $\bar{b}$ limits.

Small $\bar{b}$ limit. In the limit of small $\bar{b}$, it is found that:

$$\bar{t}^{(0)} = \beta_i \bar{b}^2 + O(\bar{b}^4), \tag{57}$$

where β_i is a material parameter characterizing the initial growth of $\bar{t}^{(0)}$ with $\bar{b}$, such that:

$$\beta_{\rm i} = \frac{1}{2}\frac{\partial^2 \bar{t}^{(0)}}{\partial \bar{b}^2}\bigg|_{\bar{b}=0} = \frac{\left(\tilde{\chi}_{\rm i}^{(0)}\right)^2 D^{(0)}(w)}{\mu_0}. \tag{58}$$

In addition, in the limit of small $\bar{b}$, it is also found that:

$$\widetilde{E}^{\rm tot} = \widetilde{E}^{\rm me} + o(\bar{b}^2), \tag{59}$$

so that the effective modulus reduces to the purely mechanical modulus in this limit.

Large $\bar{b}$ limit. As previously noted, the applied traction in Eq. (53) depends only on the magnetic fields through the magnetization; therefore in the limit of large $\bar{b}$, the magneto-mechanical effects must also saturate. The saturation value of the traction, $\bar{t}_{\rm s}$, depends on the strain, and can be written as:

$$\bar{t}_{\rm s} = \lim_{\bar{b}\to\infty} \bar{t} = \bar{t}_{\rm s}^{(0)} + \widetilde{E}_{\rm s}^{\rm tot}\bar{\epsilon}, \tag{60}$$

where $\bar{t}_{\rm s}^{(0)}$ and $\widetilde{E}_{\rm s}^{\rm tot}$ are the saturation values of $\bar{t}^{(0)}$ and $\widetilde{E}^{\rm tot}$, respectively. In this limit, it can be shown that:

$$\bar{t}_{\rm s}^{(0)} = \mu_0 m_{\rm s}^2 (c^{\rm I})^2 D^{(0)}(w), \tag{61}$$

while

$$\widetilde{E}_{\rm s}^{\rm tot} = \widetilde{E}^{\rm me} + \widetilde{E}_{\rm s}^{\rm mag}, \tag{62}$$

with

$$\widetilde{E}_{\rm s}^{\rm mag} = \mu_0 m_{\rm s}^2 (c^{\rm I})^2 D^{(1)}(w), \tag{63}$$

where

$$\begin{aligned} D^{(1)}(w) &= \left(-\frac{\partial P_1^{\rm D}}{\partial \bar{\lambda}_1 \partial \bar{\lambda}_1} + 2\frac{\partial P_1^{\rm D}}{\partial \bar{\lambda}_1 \partial \bar{\lambda}_2} - \frac{1}{2}\frac{\partial P_1^{\rm D}}{\partial \bar{\lambda}_2 \partial \bar{\lambda}_2} - \frac{1}{2}\frac{\partial P_1^{\rm D}}{\partial \bar{\lambda}_3 \partial \bar{\lambda}_2} - \frac{\partial P_1^{\rm D}}{\partial \bar{\lambda}_1} - \frac{1}{2}\frac{\partial P_1^{\rm D}}{\partial \bar{\lambda}_2}\right)\bigg|_{\bar{\lambda}_1=\bar{\lambda}_2=\bar{\lambda}_3=1} \\ &= \begin{cases} \dfrac{-8+251w^2+299w^4-2w^6}{32(-1+w^2)^3} + \dfrac{3w(7+125w^2+48w^4)\arccos(w)}{32(1-w^2)^{7/2}} & w<1 \\ -3/35 & w=1. \\ \dfrac{-8+251w^2+299w^4-2w^6}{32(-1+w^2)^3} - \dfrac{3w(7+125w^2+48w^4)\operatorname{arccosh}(w)}{32(-1+w^2)^{7/2}} & w>1 \end{cases} \end{aligned} \tag{64}$$

4.3. Magnetostriction

For magnetically susceptible materials, the magnetostrictive strain, $\bar{\epsilon}^{\rm m}$ is a very important property. It corresponds to the magnetically induced deformation when no mechanical traction is applied. An expression for the magnetostrictive strain is obtained by setting $\bar{t} = 0$ in Eq. (53), and solving for $\bar{\epsilon}$, with the result that:

$$\bar{\epsilon}^{\rm m}(\bar{b}) = \frac{-\bar{t}^{(0)}(\bar{b})}{\widetilde{E}^{\rm me} + \widetilde{E}^{\rm mag}(\bar{b})}. \tag{65}$$

However, Eq. (65) must be consistent with the small-strain approximation. The terms $\bar{t}^{(0)}$ and $\widetilde{E}^{\rm mag}$ can be shown to be of the same order of magnitude, and the small-strain requirement implies that $\bar{t}^{(0)}$ and $\widetilde{E}^{\rm mag}$ must be assumed to be small compared to $\widetilde{E}^{\rm me}$. Since $\bar{t}^{(0)}$ saturates to $\bar{t}_{\rm s}^{(0)}$, the strain will be small for all magnetic fields provided that:

$$\left|\frac{-\bar{t}_{\rm s}^{(0)}}{\widetilde{E}^{\rm me}}\right| = \frac{\mu_0 m_{\rm s}^2 (c^{\rm I})^2 \left|D^{(0)}(w)\right|}{3\widetilde{G}_{\rm a}} \ll 1. \tag{66}$$

Table 1
Typical values of κ for different constituent materials (Kaye and Laby Tables of Physical and Chemical Constants, 2011).

Matrix	G (MPa)	Inclusions	$\mu_0 m_{\rm s}$ (Tesla)	κ
Elastomer	0.01–10	High purity iron	2.16	371–.370
Elastomer	0.01–10	Cast iron	1.70	230–.230
Elastomer	0.01–10	Nickel alloys	0.77	47.2–.0472
Elastomer	0.01–10	Cobalt–iron alloy	2.35	439–.439
Silicon rubber	0.1	Steels	2.00–2.15	31.8–36.8

This condition is satisfied when the dimensionless parameter:

$$\kappa = \frac{\mu_0}{G} m_{\rm s}^2 \tag{67}$$

is small enough. The parameter κ relates the magnetic forces among the particles at saturation to the stiffness of the matrix. Higher values for κ indicate strong magnetic effects relative to the stiffness of the matrix. For known magnetic materials, $\mu_0 m_{\rm s} \leqslant 2.44T$, but κ can still be large if the matrix is soft enough (i.e., G is small), see Table 1.

When κ is such that condition (66) is satisfied, Eq. (65) reduces to:

$$\bar{\epsilon}^{\rm m}(\bar{b}) = \frac{-\bar{t}^{(0)}(\bar{b})}{\widetilde{E}^{\rm me}}. \tag{68}$$

More explicit expressions can then be obtained in the limits of small and large $\bar{b}$, as given next.

Small $\bar{b}$ limit. In this limit, $\bar{t}^{(0)}$ is given by expression (57), and it follows that:

$$\bar{\epsilon}^{\rm m}(\bar{b}) = \alpha_{\rm i}\bar{b}^2 + o(\bar{b}^4), \tag{69}$$

where

$$\alpha_{\rm i} = \frac{1}{2}\frac{\partial^2 \bar{\epsilon}^{\rm m}}{\partial \bar{b}^2}\bigg|_{\bar{b}=0} = \frac{-\left(\tilde{\chi}_{\rm i}^{(0)}\right)^2 D^{(0)}(w)}{3\mu_0 \widetilde{G}_{\rm a}}, \tag{70}$$

is a parameter describing $\bar{\epsilon}^{\rm m}$ in the linear magnetization regime, where, according to (69), $\bar{\epsilon}^{\rm m}$ grows quadratically with $\bar{b}$.

Large $\bar{b}$ limit. For large $\bar{b}$, the magnetization saturates and $\bar{\epsilon}^{\rm m}$ is given by

$$\bar{\epsilon}_{\rm s}^{\rm m} = \lim_{\bar{b}\to\infty} \bar{\epsilon}^{\rm m} = \frac{-\bar{t}_{\rm s}^{(0)}}{3\widetilde{G}_{\rm a}} = \frac{-\mu_0 m_{\rm s}^2 (c^{\rm I})^2 D^{(0)}(w)}{3\widetilde{G}_{\rm a}}, \tag{71}$$

which is proportional to κ and to the square of the volume fraction $c^{\rm I}$ (for small $c^{\rm I}$).

4.4. Actuator energy density

The actuation stress $\bar{t}_{\rm s}^{(0)}$ and the magnetostriction $\bar{\epsilon}_{\rm s}^{\rm m}$ are both important measures of actuator performance. However, in applications, the actuation energy density, describing the potential for energy transfer, is often more important (Pelrine et al., 2000).

At saturation, the actuation energy density for the uniaxial loading conditions of this section can be estimated as:

$$\bar{e}_{\rm a} = \left|\bar{\epsilon}_{\rm s}^{\rm m}\bar{t}_{\rm s}^{(0)}\right| = \frac{\mu_0^2 m_{\rm s}^4 (c^{\rm I})^4 (D^{(0)}(w))^2}{3\widetilde{G}_{\rm a}}, \tag{72}$$

which can also be written in terms of the parameter κ as:

$$\bar{e}_{\rm a} = \kappa\mu_0 m_{\rm s}^2 \frac{G}{3\widetilde{G}_{\rm a}} (c^{\rm I})^4 (D^{(0)}(w))^2. \tag{73}$$

This means that, for combinations of G and $m_{\rm s}$ resulting in the same κ, the energy density is maximized for the largest value of $m_{\rm s}$. Also,

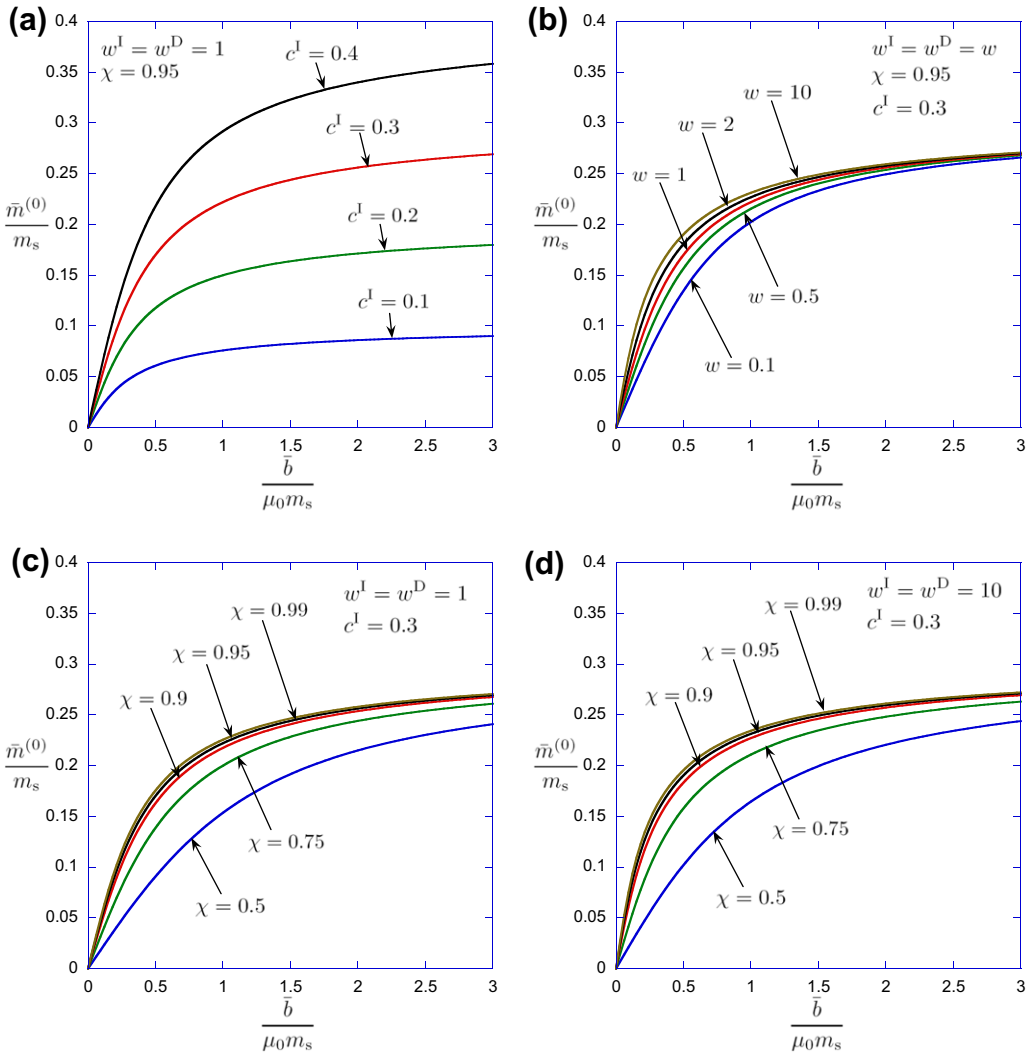

Fig. 3. The magnetization in the unstrained composite $\bar{m}^{(0)}(\bar{b})$ as a function of magnetic flux $\bar{b}$ for various microstructures. (a) The magnetization curves for various concentrations c^{I} with spherical aspect ratio $w = 1$. (b) The curves for a fixed concentration c^{I} and a variety of aspect ratios w. (c) The magnetization curves for spherical aspect ratios $w = 1$ for different particle susceptibilities χ. (d) The magnetization curves for elongated aspect ratios $w = 10$ for different particle susceptibilities χ.

note that, at saturation, the energy transfer is proportional to the volume fraction c^{I} to the fourth power (for small c^{I}).

5. Discussion of the results for uniaxial loading

Fig. 3 shows the magnetization curves for the composite when $\bar{\epsilon} = 0$, as determined by the nonlinear variational estimate (Eqs. (35)–(38)). The plots are normalized by the magnetic saturation m_{s}. The initial slope of these curves is $\tilde{\chi}_{\mathrm{i}}^{(0)}$ and the value as $\bar{b} \to \infty$ is the magnetic saturation $\bar{m}_s$. Fig. 3(a) shows how the saturation magnetization and the initial susceptibility increase with the inclusion concentration. In agreement with expression (51), the results show that the saturation magnetization scales linearly with the concentration, while the initial susceptibility has a more complicated dependence on concentration. On the other hand, Fig. 3(b) shows that the initial susceptibility of the composite has a marked dependence on particle shape, while the saturation magnetization is independent of particle shape. Fig. 3(c) and (d) depict the effect of particle initial susceptibility χ on the properties of the composite. Examining both plots we can see that changing the initial susceptibility of the particles affects the initial susceptibility of the composite, but not the corresponding saturation values.

Fig. 4 shows more detailed plots of the effect of microstructure on the zero-strain initial susceptibility of the composite $\tilde{\chi}_{\mathrm{i}}^{(0)}$. Elongated initial shapes ($w > 1$) lead to larger initial susceptibilities for the composite. This makes sense because elongated, isolated particles (with $w > 1$) magnetize more easily than disk shaped particles (with $w < 1$). The composite susceptibility also depends on the particle susceptibility, but the focus here is on values of χ close to 1, where the change in χ has a relatively small effect on the behavior of the composite. The effect of the strain $\bar{\epsilon}$ on the initial susceptibility $\tilde{\chi}_{\mathrm{i}}$ may be obtained via expression (47), but is relatively small and will not be shown here. Also, as already mentioned, the strain $\bar{\epsilon}$ has no effect on the saturation magnetization of the composite.

Fig. 5 depicts the effects of the magnetic field on the traction-strain curve. The traction is non-dimensionalized by the shear modulus of the matrix phase. Fig. 5(a) shows the magnetic field has the effect of shifting the curve downwards; essentially, this means that a compressive traction would be necessary to prevent the sample from elongating. The value of this traction is specified by the vertical intercept of the curves and is the actuation stress $\bar{t}^{(0)}$. The corresponding horizontal displacement defines the magnetostrictive strain, $\bar{\epsilon}^{\mathrm{m}}$. As the magnetic field increases, the plots approach the saturation traction-strain curve whose vertical and horizontal intercepts are $\bar{t}_{\mathrm{s}}^{(0)}$ and $\bar{\epsilon}_{\mathrm{s}}^{\mathrm{m}}$ respectively. These plots were

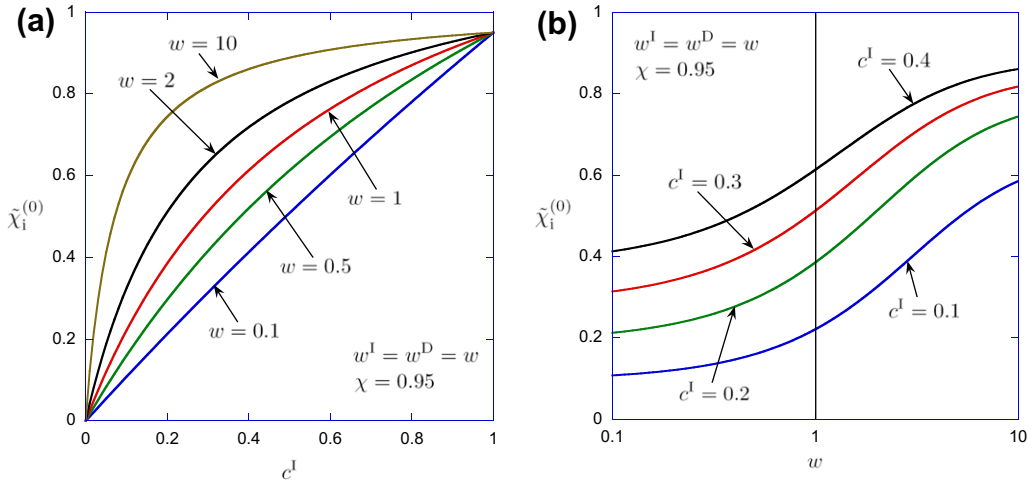

Fig. 4. The initial susceptibility of the unstrained composite $\tilde{\chi}_{\mathrm{i}}^{(0)}$ for different microstructures. The particle initial susceptibility is $\chi = 0.95$. (a) $\tilde{\chi}_{\mathrm{i}}^{(0)}$ as a function of concentration c^{I}. (b) $\tilde{\chi}_{\mathrm{i}}^{(0)}$ as a function of aspect ratio w.

obtained neglecting the contribution of $\widetilde{E}^{\mathrm{mag}}(\bar{b})$ because the effect of $\widetilde{E}^{\mathrm{mag}}(\bar{b})$ is small, as we will show. Fig. 5(b) shows the effect of increasing κ on the saturation traction-strain curves. As expected for larger κ, there is a more pronounced effect of the magnetic field indicating that the magnetic effects are stronger compared to the mechanical effects.

The plots in Fig. 6 show the traction as a function of the strain for $\kappa = 16$. The plots are for $\bar{b} = 0$ and $\bar{b} \to \infty$. The different slopes in Fig. 6(a) and (c) illustrate the mechanical reinforcement effect of the particles on the composite. They depend on the particle shape and concentration. Fig. 6(b) and (d) show the corresponding plots when a magnetic field is applied. The slope of the curve remains the same but there is a shift downwards. The vertical shift increases monotonically with concentration, but shows a more complex dependence on the particle aspect ratio. There is a very small change in the slope of the curves due to the magnetic field, which is not visible here, but will be discussed next when we look at the modulus curves.

Fig. 7 depicts the magnetoelastic moduli of the composite at high magnetic field normalized by the shear modulus of the matrix. The total modulus $\widetilde{E}_{\mathrm{s}}^{\mathrm{tot}}$ depends on the magnetic field, but $\widetilde{E}_{\mathrm{s}}^{\mathrm{mag}}$ is small relative to the mechanical contribution even though the magnetic field is large enough to bring all the particles to saturation. Thus, the primary effects seen in Fig. 7(a) and (c) are the role of aspect ratio w and concentration c^{I} on the purely mechanical reinforcement of the composite. It is interesting that even though the magnetic modulus is small, it can be negative or positive depending on particle aspect ratio, as shown in Fig. 7(b) and (d). This magnetic modulus is due to the magnetic forces on particles changing relative positions with the deformation. These particle forces depend in a complicated way on the microstructure; subsequently, the modulus depends on how the microstructure changes with the deformation. In principle we could also consider fixed **m**, fixed **h**, and fixed **b** moduli which would be different for magnetic fields below saturation; however since the magnetic field would be smaller the overall effect would also be minimal.

Fig. 8 shows the magnetostriction $\bar{\epsilon}^{\mathrm{m}}$ as a function of $\bar{b}$ for different aspect ratios w and concentrations c^{I}. The magnetostriction is normalized by κ indicating that, for fixed microstructure, magnetostriction is a balance between the magnetic saturation of the particle and the stiffness of the matrix, and can be increased by softening the matrix. The effect is initially quadratic in $\bar{b}$ but then saturates. The range of $\bar{b}$ where the magnetostriction is quadratic is the range where the magnetization is linear. The initial curvature

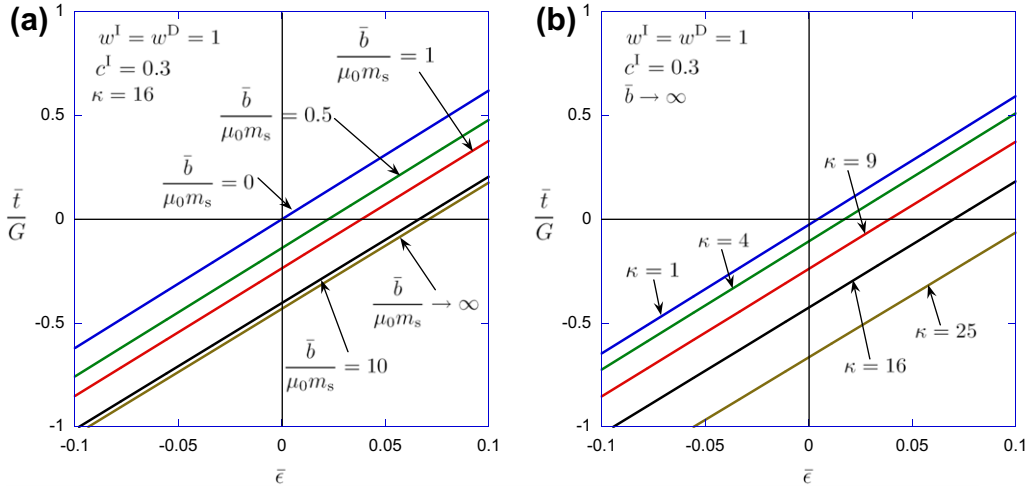

Fig. 5. The traction $\bar{t}$ as a function of the strain $\bar{\epsilon}$ for different magnetic loadings and material parameters. (a) The traction-strain curves for different magnetic flux $\bar{b}$. (b) The saturation traction-strain curves for different values of κ.

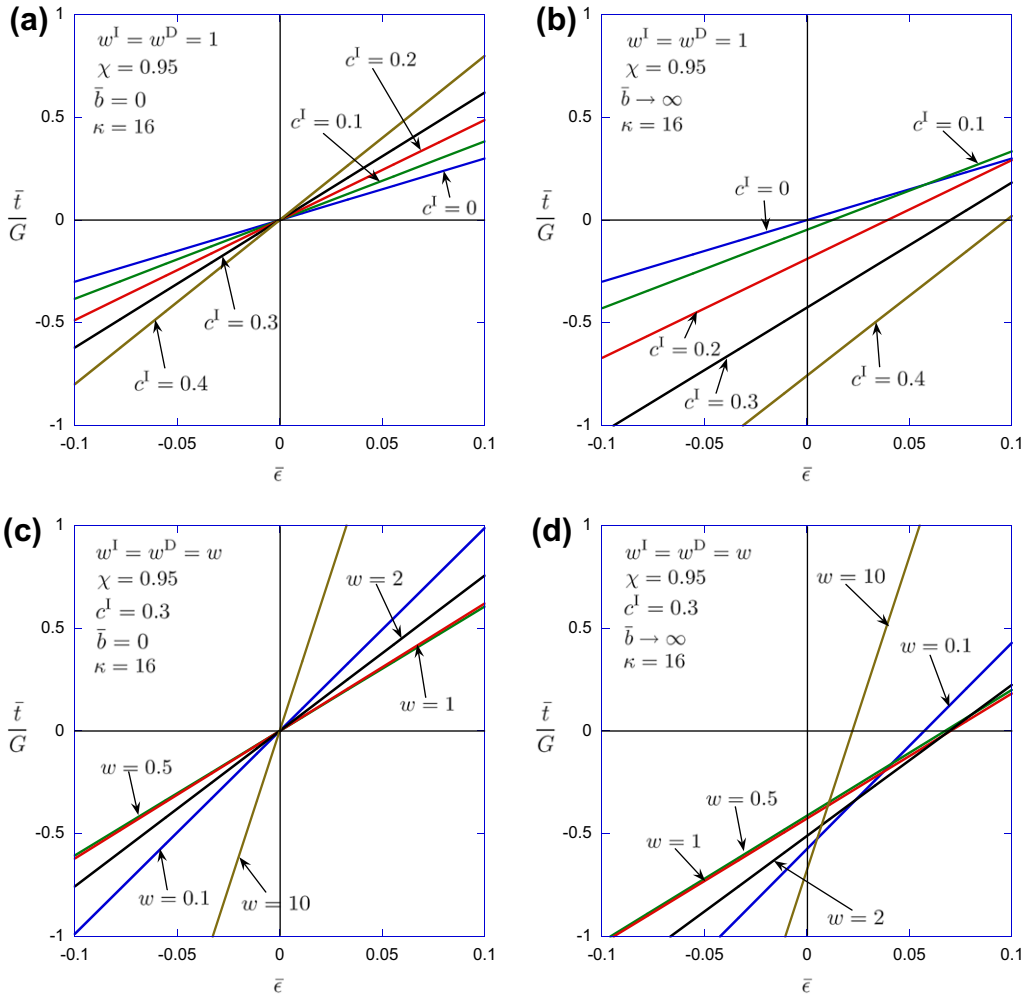

Fig. 6. The traction $\bar{t}$ vs strain $\bar{\epsilon}$ with no magnetic field and with high magnetic field $\bar{b} \to \infty$. (a) The traction-strain curves for spherical aspect ratio $w = 1$ at different concentrations c^I when the magnetic field is off. (b) Corresponding plots when the magnetic field is large enough to saturate the composite. (c) The traction-strain curves for $c^I = 0.3$ and different aspect ratios w when the magnetic field is off. (d) Corresponding plots when the magnetic field is large enough to saturate the composite.

of the lines is determined by the parameter α_i, defined by (70), and the limiting value of magnetostriction by $\bar{\epsilon}_s^m$, defined by (71). The predicted effect is always extension in the direction of the applied magnetic field regardless of aspect ratio and concentration. This is confirmed by experiments on spherical particles (Ginder et al., 2002; Guan et al., 2008).

The plots in Fig. 9 show the effect of concentration c^I and the aspect ratio w on the initial and saturation behavior of magnetostriction. Plots Fig. 9(a) and (c) characterize the magnetostriction when the composite is magnetically linear, while plots Fig. 9(b) and (d) show the magnetostriction at saturation. The two effects are clearly different. The saturation magnetostriction depends on the distribution of the particles, the saturation magnetization, and the mechanical reinforcement. For fixed concentration, the mechanical reinforcement is minimized for aspect ratios below 1(b) so the maximum $\bar{\epsilon}_s^m$ is obtained when $c^I \approx 0.61$ and $w \approx 0.67$. The initial behavior depends on the same parameters and on the composite susceptibility. The composite susceptibility is larger for elongated particles, $w > 1$, which initially leads to large magnetostriction despite the additional stiffening effect. Both effects tend to vanish as $c^I \to 1$ or w is far from 1 because the composite is becoming mechanically rigid. Overall, for fixed κ, magnetostriction is maximized by increasing the magnetic forces produced by the inclusions and minimizing their reinforcement of the composite.

Fig. 10 shows the actuation stress $\bar{t}^{(0)}$ normalized by $\mu_0 m_s^2$ as a function of $\bar{b}$ for different aspect ratios w and concentrations c^I. The effect is initially quadratic in $\bar{b}$ but then saturates as $\bar{b}$ becomes large. The range of $\bar{b}$ where the actuation stress is quadratic is the range where the magnetization is linear. The initial curvature of the lines is the parameter β_i and the limiting value of actuation stress is $\bar{t}_s^{(0)}$, as given by expressions (58) and (61), respectively. These curves are independent of the matrix and the mechanical stiffening. They correspond to a property of the initial configuration of magnetic particles and represent the net magnetic force generated by the current distribution of magnetic particles.

The plots in Fig. 11 show the effect of the concentration c^I and aspect ratio w on the initial and saturation behaviors of the actuation stress. Plots Fig. 11(a) and (c) characterize the actuation stress when the composite is magnetically linear, while plots Fig. 11(b) and (d) show the actuation stress at saturation. $\bar{t}_s^{(0)}$ is quadratic in the concentration because it depends only on the saturation magnetization and the distribution of the particles. It is not compensated for by the mechanical reinforcement like the magnetostriction. In the range of linear magnetic behavior, the composite susceptibility also affects the actuation stress which leads to the more complicated behavior for β_i. Prolate shapes (with $w > 1$) tend to have a bigger effect on β_i than oblate shapes (with $w < 1$), but both prolate and oblate shapes tend to increase the saturation traction $|\bar{t}_s^{(0)}|$. This indicates that both prolate and oblate shapes can

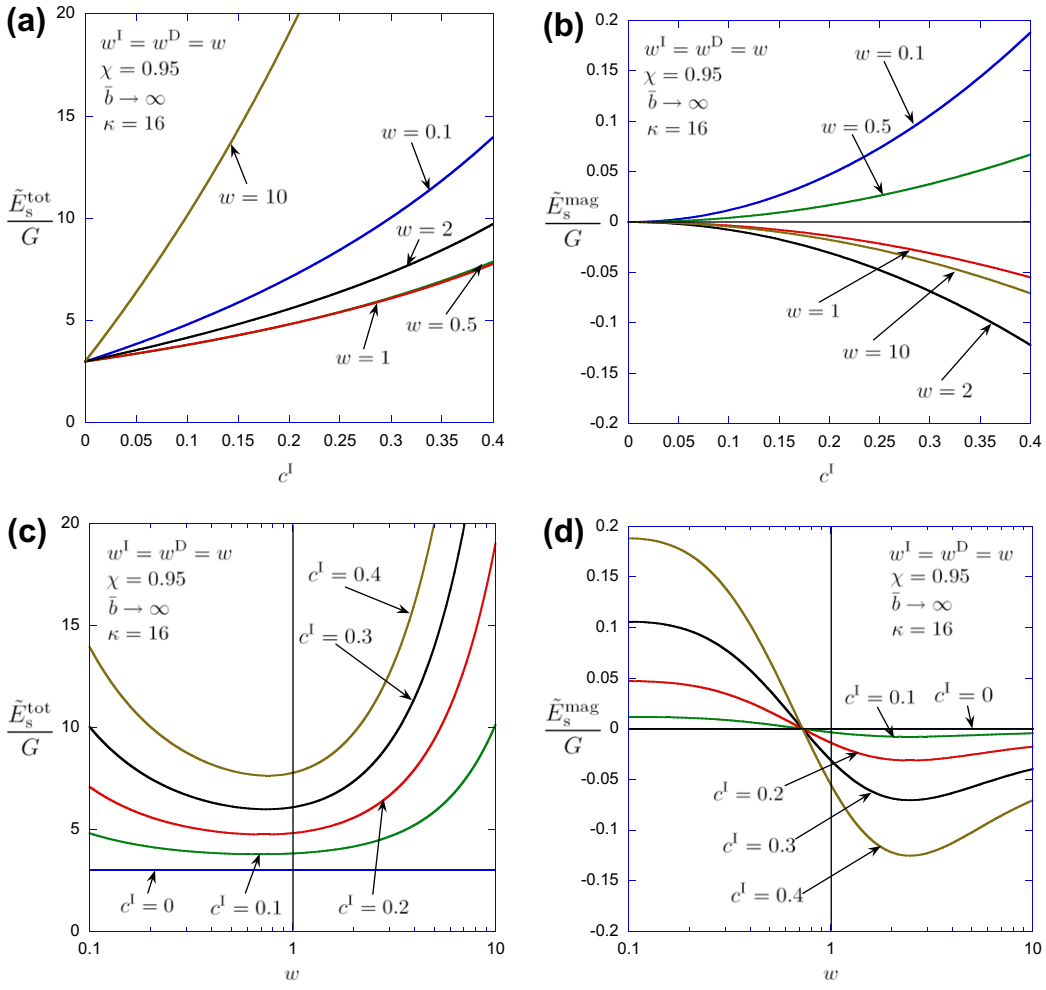

Fig. 7. The total magnetoelastic Young's modulus $\tilde{E}_{\mathrm{s}}^{\mathrm{tot}}$ and the magnetic contribution to the modulus $\tilde{E}^{\mathrm{mag}}$ when the field is large enough to bring all the particles to saturation. (a) The total Young's modulus of the composite as a function of concentration c^{I}. (b) The corresponding magnetic part of the Young's modulus. (c) The total Young's modulus of the composite as a function of aspect ratio w. (d) The corresponding magnetic part of the Young's modulus.

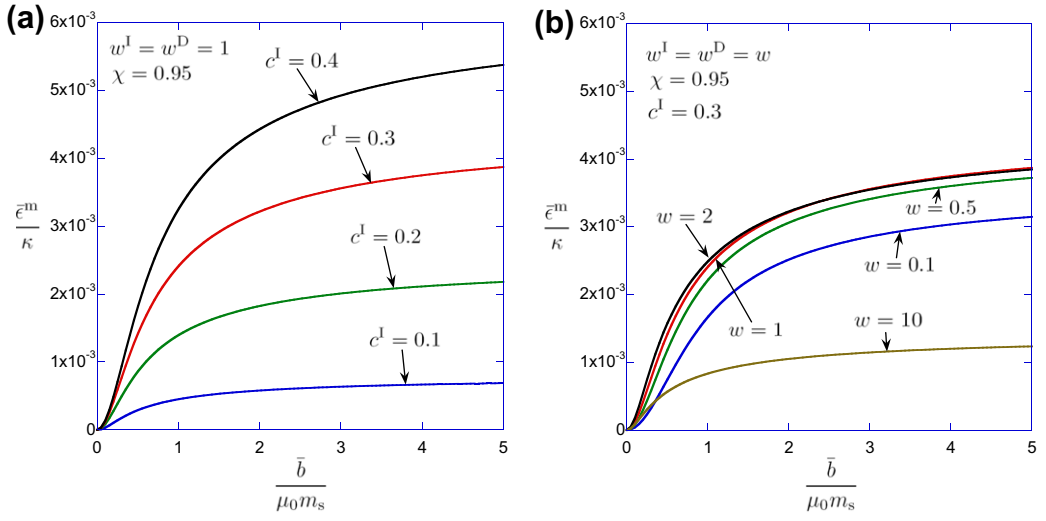

Fig. 8. The magnetostriction $\bar{\epsilon}^{\mathrm{m}}$ as a function of the applied magnetic field $\bar{b}$ for different microstructures. (a) The magnetostriction for different concentrations c^{I} with spherical aspect ratio $w = 1$. (b) The magnetostriction for different aspect ratios w and concentration $c^{\mathrm{I}} = 0.3$.

lead to a greater actuation stress, but in the linear regime oblate shapes are slower to magnetize, limiting the actuation stress of the composite.

Fig. 12 shows the actuation energy density $\bar{e}_a$ as a function of the concentration c^{I} and aspect ratio w. The actuation energy density is quartic to leading order in the concentration, so that even for

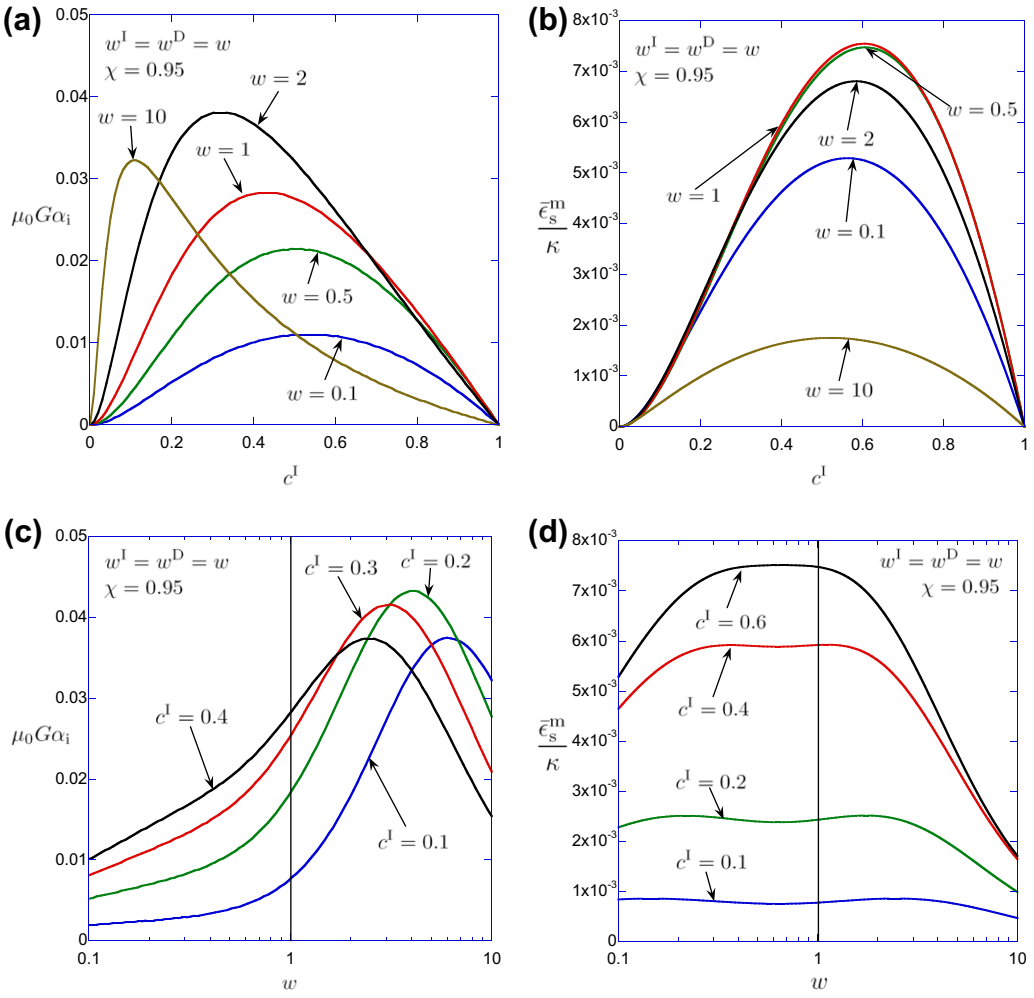

Fig. 9. The coefficient of magnetostriction α_i and the saturation magnetostriction $\bar{\epsilon}_s^m$ for different microstructures. The results correspond to the magnetostriction in the range of linear magnetization and the saturation magnetization. (a) The coefficient of magnetostriction α_i and (b) the saturation magnetostriction $\bar{\epsilon}_s^m$ as a function of the concentration c^I. (c) The coefficient of magnetostriction α_i and (d) the saturation magnetostriction $\bar{\epsilon}_s^m$ as a function of the aspect ratio w.

concentrations up to 40%, it is relatively small. The dependence on the aspect ratio is more subtle, showing that for a set concentration there are two local maxima for the energy density. This effect is the result of a complex dependence on the magnetic and mechanical properties of the composite. The actuation energy also goes to zero when $c^I \to 1$ or w is far from 1 because the composite is becoming mechanically rigid. On the other hand, when $c^I = 0$, the magnetic energy is unavailable to the composite because the magnetization vanishes.

Fig. 13 provides a comparison of the predictions of the theory against the experiments of Guan et al. (2008), for the magnetostriction $\bar{\epsilon}^m$ as a function of the magnetic intensity $\bar{h}$. Even though the precise material properties for the matrix and particles were not provided by the authors, it was still possible to infer values of the properties in our model to achieve a reasonable match to the experimental data. The model does predict a somewhat weaker effect of particle concentration than the experiments. This is consistent with the use of estimates of the Hashin–Shtrikman type for the magnetic and elastic effects, which are known to underestimate the effect of particle interactions, especially at large volume fractions. However, given the uncertainties involved in the experimental data, the model does capture very well the qualitative features of the experiments, and can even provide reasonably good predictive capabilities. In addition, it should be noted that Guan et al.'s experiments exhibited hysteresis, which is not accounted for in our theory. The hysteresis of the particles themselves is very difficult to describe and including these effects in the homogenization is beyond the scope of the present work.

It is also relevant to mention that Diguet et al. (2010) have measured experimentally the magnetostriction of a cylinder made of an MRE. However, their results depend on the aspect ratio of the cylinder (which is not the same as the aspect ratio of the inclusions) and do not correspond to the magnetostriction defined in this paper, which is a shape-independent (i.e., a material) property. However the results are qualitatively consistent and of the same order of magnitude.

6. Concluding remarks

In this work, estimates have been developed for the magneto-elastic properties of spheroidal-particle MREs under aligned loading conditions. The properties include the magnetostrictive strain, the field-dependent Young's modulus, the actuation stress, and the actuation energy density. The results are based on the finite-strain homogenization framework and partial decoupling approximation introduced in Ponte Castañeda and Galipeau (2011), which provides estimates for the total stress and magnetization in MREs with rigid magnetic inclusions. In particular, expressions for the applied traction on the composite are derived from the total stress by accounting for the magnetic stress outside the sample. The results are formulated in the finite strain context,

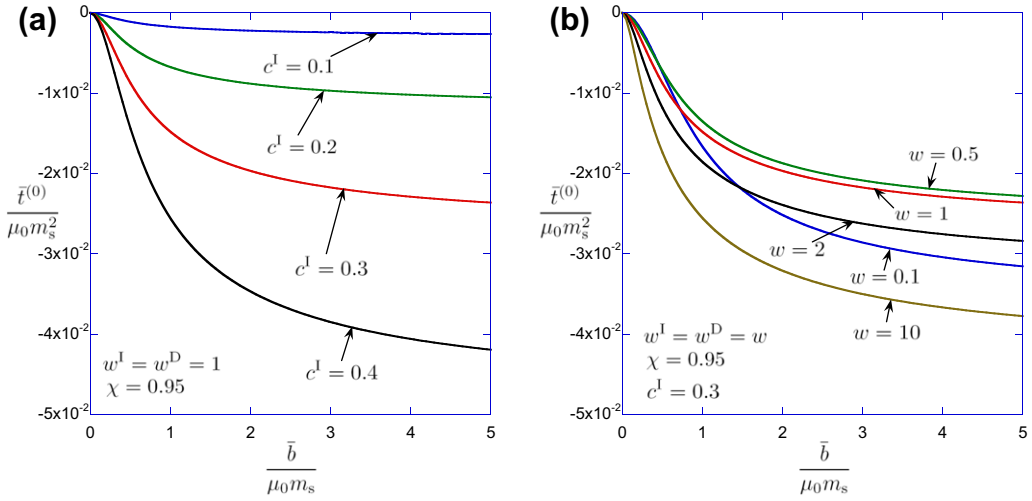

Fig. 10. The actuation stress $\bar{t}^{(0)}$ as a function of the applied magnetic field $\bar{b}$ for different microstructures. (a) The actuation stress $\bar{t}^{(0)}$ for different concentrations c^{I} with spherical aspect ratio $w = 1$. (b) The actuation stress $\bar{t}^{(0)}$ for different aspect ratios w and concentration $c^{\mathrm{I}} = 0.3$.

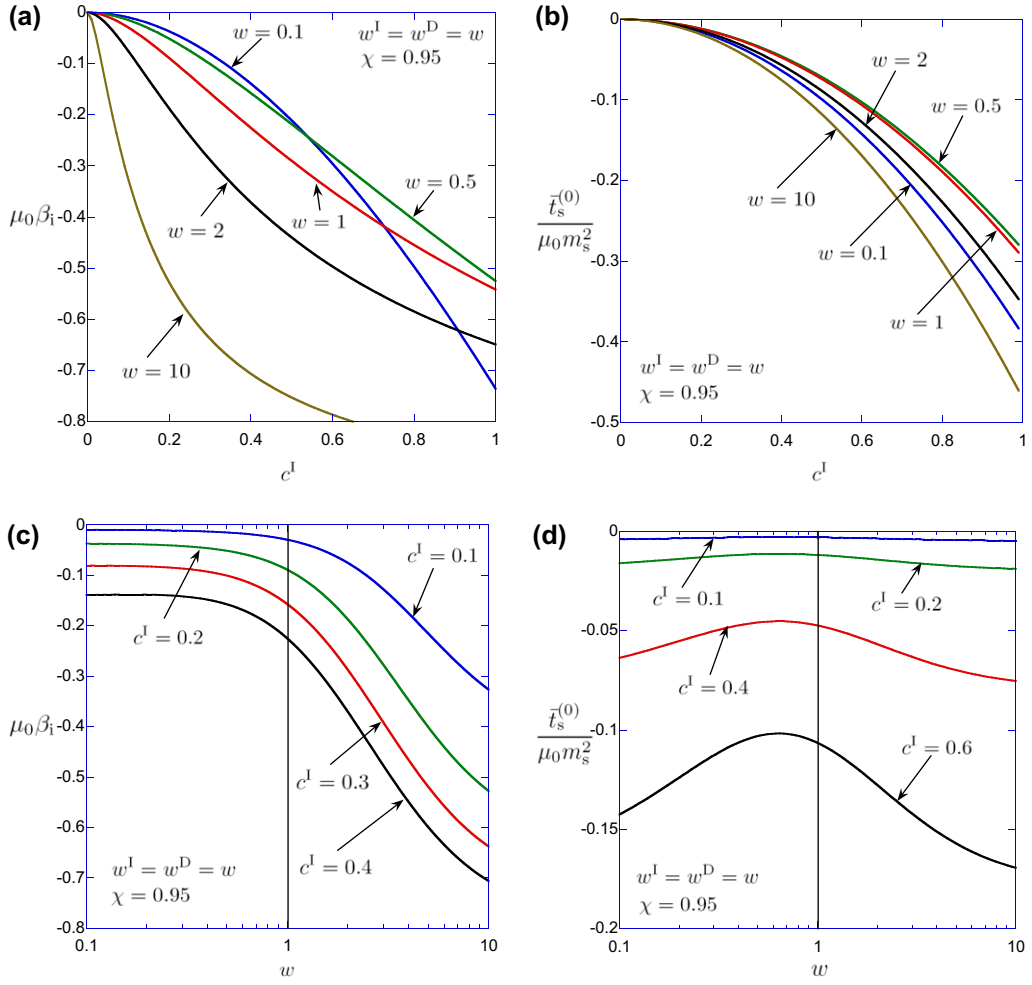

Fig. 11. The coefficient of actuation stress β_i and the saturation actuation stress $\bar{t}_{\mathrm{s}}^{(0)}$ for different microstructures. The results correspond to the actuation stress in the range of linear magnetization and the saturation actuation stress. (a) The coefficient of actuation stress β_i and (b) the saturation actuation stress $\bar{t}_{\mathrm{s}}^{(0)}$ as a function of the concentration c^{I}. (c) The coefficient of actuation stress β_i and (d) the saturation actuation stress $\bar{t}_{\mathrm{s}}^{(0)}$ as a function of the aspect ratio w.

but then specialized for small strains, where we define appropriate parameters characterizing the magnetoelastic behavior of the composites.

The magnetoelastic effects in these systems are found to be of second order in the particle concentration and limited by the magnetic saturation of the particles. In this context, it should be

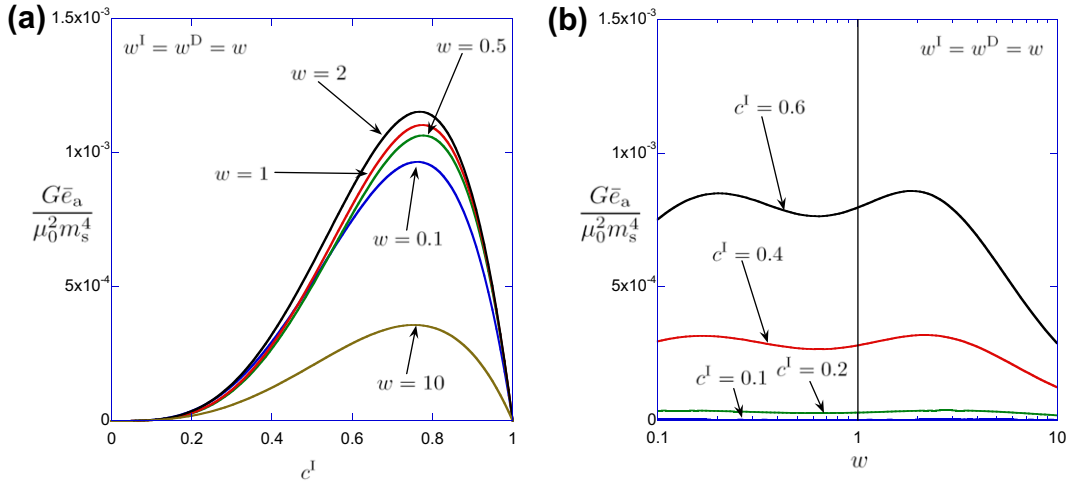

Fig. 12. The actuation energy density $\bar{e}_a$ for different microstructures. (a) Actuator energy density $\bar{e}_a$ as a function of concentration c^{I}. (b) Actuator energy density $\bar{e}_a$ as a function of aspect ratio w.

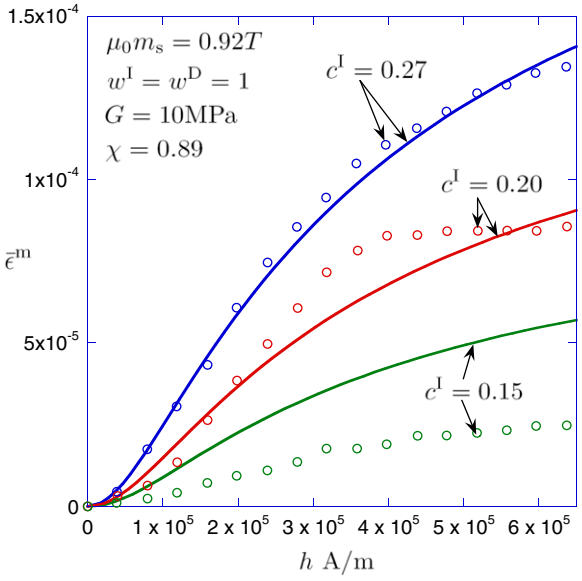

Fig. 13. The predicted magnetostriction $\bar{\epsilon}^{\mathrm{m}}$ as a function of $\bar{h}$ compared against the experimental results of Guan et al. (2008). The solid lines are theoretical results and the discrete values are the experimental results. The experimental materials exhibit hysteresis so the plot compares the initial loading vs. the theoretical results.

emphasized that while the macroscopic stress inside a given MRE specimen includes contributions that are of first order in the concentration, such contributions drop out from the corresponding expressions for the external traction (on the specimen), because of the Maxwell stresses that surround the specimen. This result is consistent with the fact that for small (dilute) concentrations, the particles do not interact and the net forces on the particles vanish, producing no magnetoelastic coupling effects. In addition, the magnetoelastic coupling is seen to arise from the dependence of the (nonlinear) magnetic susceptibility of the MRE on the deformation, and has been linked to certain microstructural tensors characterizing the two-point correlation function for the random distribution of the particles in the elastomer matrix. However, the thermodynamically consistent approach followed in this work is different from earlier approaches (Borcea and Bruno, 2001; Yin and Sun, 2006), which estimated the average stress in the composite by means of a direct computation of the inter-particle forces. Although the specific results developed in this work made use of variational estimates (Ponte Castañeda and Willis, 1995) incorporating up to two-point statistics for the distribution of the particle in the composite, the method is more general and could, in principle, be generalized to include the effects of higher-order statistics, to obtain more accurate estimates at higher particle concentrations.

Concerning the specific results of this work, it is important to distinguish between two different regimes: the linear magnetization regime and the saturation magnetization regime. In the linear regime, the magnetoelastic coupling is largely controlled by the composite susceptibility, with microstructures that magnetize easily favoring strong magnetoelastic effects. In the saturation regime, the effects are controlled by the saturation magnetization of the particles and their distribution in space. For small applied magnetic fields $\bar{b}$, the magnetostrictive strain grows quadratically with $\bar{b}$. The corresponding coefficient increases and then decreases with the particle concentration and aspect ratio (from oblate to prolate shapes), reaching a maximum effect for a particle concentration of about 0.2 and a prolate particle shape with aspect ratio of about 4. On the other hand, for large values of $\bar{b}$, the effect saturates and scales with the dimensionless parameter $\kappa = \mu_0 m_s^2/G$, characterizing the relative strengths of the magnetic to the elastic forces in the MRE systems. The maximum magnetostrictive strain is reached at saturation for a particle concentration of about 0.61 and an oblate particle shape with aspect ratio of about 0.67. These different results for different regimes demonstrate clearly the need to account for the magnetic nonlinearity of the material when seeking to optimize the microstructure in these MRE systems. Predictions for the optimal microstructure based on the (linear) magnetic susceptibility of the material do not continue to hold when the magnetic saturation of the particles – corresponding to the largest possible magnetostrictive strain that the composite material can sustain – is accounted for. Corresponding predictions for the actuation stress (at saturation) show that the effect is enhanced by larger concentrations of particles and by both strongly oblate and prolate shapes. Now, while the optimal microstructures for the magnetostrictive strain and the actuation stress are somewhat contradictory, in applications, a more useful figure of merit is the actuation energy density of the material, which is found to be optimized by relatively large volume fractions in the order of 75% and either slightly prolate shapes, or somewhat oblate shapes (with aspect ratios of 2 and 0.2, respectively). Finally, the effect of the magnetic field on the Young's modulus of the material was found to be relatively small compared to the purely mechanical modulus of the compos-

ite, although it is worth emphasizing that prolate shapes can be used to reduce the total modulus of the MRE under application of a magnetic field.

The results presented in this paper have focused on magnetic and mechanical loadings that are aligned with the uniaxial symmetry axes of the particles. We have also considered magnetic loadings that are perpendicular to this symmetry axis, and investigated the effects of particle distributions in an attempt to model chain distributions of spherical particles. However, the characterization of such systems requires consideration of more general orthotropic symmetries for the material behavior, leading to significantly more complex expressions and results, which will be reported elsewhere (Galipeau, 2012). More generally, if the magnetic and/or mechanical loading axis are not aligned with the particle axes, additional effects are expected due to the particle rotations that would be generated by the magnetic and elastic torques on the particles. The particle rotations generated by a non-aligned magnetic field have been addressed recently by Siboni and Ponte Castañeda (2011a) in the context of small strains and rotations. Such particle rotations, whether induced mechanically or magnetically, have been shown to produce effects that are of the same order as the particle concentration, and a dilute theory has been developed accordingly by Siboni and Ponte Castañeda (2011b), again in the small strain/small rotation context. More general calculations in the context of finite deformations for non-aligned situations are in progress and will be reported elsewhere (Galipeau and Ponte Castañeda, in preparation).

Finally, it should be noted that the results of this work concerning the effects of particle shape for MREs are also expected to be relevant for certain types of dielectric elastomer composites. Indeed, it has been shown recently (Ponte Castañeda and Siboni, 2011) that the framework of Ponte Castañeda and Galipeau (2011) for magnetoelastic composites can be extended to certain classes of electroactive polymer composites consisting of stiff dielectric (ferroelectric) particles that are randomly distributed in a soft dielectric elastomer matrix that can be idealized as having a deformation-independent dielectric coefficient.

Acknowledgements

This work has been supported by the National Science Foundation under Grant DMS-0708271.

Appendix A. The derivatives of P^{D}.

In this appendix, we provide the derivatives of the distribution tensor $\boldsymbol{P}^{\mathrm{D}}(\boldsymbol{U})$, evaluated when $\bar{\lambda}_1 = \bar{\lambda}_2 = \bar{\lambda}_3 = 1$, for spheroidal distributions aligned with the $\hat{\mathbf{e}}_1$ axis. Note that in these expressions $w = w^{\mathrm{D}}$.

$$\left.\frac{\partial P_1^{\mathrm{D}}}{\partial \bar{\lambda}_1}\right|_{\bar{\lambda}_1=\bar{\lambda}_2=\bar{\lambda}_3=1} = \begin{cases} \dfrac{4w^2-1}{(-1+w^2)^2} - \dfrac{3w^3\arccos(w)}{(1-w^2)^{5/2}} & w<1 \\ -3/5 & w=1 \\ \dfrac{4w^2-1}{(-1+w^2)^2} - \dfrac{3w^3\operatorname{arccosh}(w)}{(-1+w^2)^{5/2}} & w>1 \end{cases},$$

$$\left.\frac{\partial P_1^{\mathrm{D}}}{\partial \bar{\lambda}_2}\right|_{\bar{\lambda}_1=\bar{\lambda}_2=\bar{\lambda}_3=1} = \left.\frac{\partial P_1^{\mathrm{D}}}{\partial \bar{\lambda}_3}\right|_{\bar{\lambda}_1=\bar{\lambda}_2=\bar{\lambda}_3=1} = \begin{cases} \dfrac{-2-w^2}{2(1-w^2)^2} + \dfrac{3w\arccos(w)}{2(1-w^2)^{5/2}} & w<1 \\ -1/5 & w=1 \\ \dfrac{-2-w^2}{2(1-w^2)^2} + \dfrac{3w\operatorname{arccosh}(w)}{2(-1+w^2)^{5/2}} & w>1 \end{cases},$$

$$\left.\frac{\partial P_2^{\mathrm{D}}}{\partial \bar{\lambda}_1}\right|_{\bar{\lambda}_1=\bar{\lambda}_2=\bar{\lambda}_3=1} = \left.\frac{\partial P_3^{\mathrm{D}}}{\partial \bar{\lambda}_1}\right|_{\bar{\lambda}_1=\bar{\lambda}_2=\bar{\lambda}_3=1} = \begin{cases} \dfrac{-2w^2-w^4}{2(-1+w^2)^2} + \dfrac{3w^3\arccos(w)}{2(1-w^2)^{5/2}} & w<1 \\ -1/5 & w=1 \\ \dfrac{-2w^2-w^4}{2(-1+w^2)^2} + \dfrac{3w^3\operatorname{arccosh}(w)}{2(-1+w^2)^{5/2}} & w>1 \end{cases},$$

$$\left.\frac{\partial P_2^{\mathrm{D}}}{\partial \bar{\lambda}_2}\right|_{\bar{\lambda}_1=\bar{\lambda}_2=\bar{\lambda}_3=1} = \left.\frac{\partial P_3^{\mathrm{D}}}{\partial \bar{\lambda}_3}\right|_{\bar{\lambda}_1=\bar{\lambda}_2=\bar{\lambda}_3=1} = \begin{cases} \dfrac{15w^2-6w^4}{8(-1+w^2)^2} - \dfrac{9w\arccos(w)}{8(1-w^2)^{5/2}} & w<1 \\ -3/5 & w=1 \\ \dfrac{15w^2-6w^4}{8(-1+w^2)^2} - \dfrac{9w\operatorname{arccosh}(w)}{8(-1+w^2)^{5/2}} & ws>1 \end{cases},$$

$$\left.\frac{\partial P_2^{\mathrm{D}}}{\partial \bar{\lambda}_3}\right|_{\bar{\lambda}_1=\bar{\lambda}_2=\bar{\lambda}_3=1} = \left.\frac{\partial P_3^{\mathrm{D}}}{\partial \bar{\lambda}_2}\right|_{\bar{\lambda}_1=\bar{\lambda}_2=\bar{\lambda}_3=1} = \begin{cases} \dfrac{5w^2-2w^4}{8(-1+w^2)^2} - \dfrac{3w\arccos(w)}{8(1-w^2)^{5/2}} & w<1 \\ -1/5 & w=1 \\ \dfrac{5w^2-2w^4}{8(-1+w^2)^2} - \dfrac{3w\operatorname{arccosh}(w)}{8(-1+w^2)^{5/2}} & w>1 \end{cases},$$

$$\left.\frac{\partial P_1^{\mathrm{D}}}{\partial \bar{\lambda}_1 \partial \bar{\lambda}_1}\right|_{\bar{\lambda}_1=\bar{\lambda}_2=\bar{\lambda}_3=1} = \begin{cases} \dfrac{-2+6w^2-19w^4}{(-1+w^2)^3} - \dfrac{3w^3(1+4w^2)\arccos(w)}{(1-w^2)^{7/2}} & w<1 \\ 54/35 & w=1 \\ \dfrac{-2+6w^2-19w^4}{(-1+w^2)^3} + \dfrac{3w^3(1+4w^2)\operatorname{arccosh}(w)}{(-1+w^2)^{7/2}} & w>1 \end{cases},$$

$$\left.\frac{\partial P_1^{\mathrm{D}}}{\partial \bar{\lambda}_2 \partial \bar{\lambda}_2}\right|_{\bar{\lambda}_1=\bar{\lambda}_2=\bar{\lambda}_3=1} = \left.\frac{\partial P_1^{\mathrm{D}}}{\partial \bar{\lambda}_3 \partial \bar{\lambda}_3}\right|_{\bar{\lambda}_1=\bar{\lambda}_2=\bar{\lambda}_3=1} = \begin{cases} \dfrac{-16-31w^2+2w^4}{8(-1+w^2)^3} - \dfrac{3w(11+4w^2)\operatorname{arccosh}(w)}{8(1-w^2)^{7/2}} & w<1 \\ 8/35 & w=1 \\ \dfrac{-16-31w^2+2w^4}{8(-1+w^2)^3} + \dfrac{3w(11+4w^2)\operatorname{arccosh}(w)}{8(-1+w^2)^{7/2}} & w>1 \end{cases},$$

$$\left.\frac{\partial P_1^{\mathrm{D}}}{\partial \bar{\lambda}_2 \partial \bar{\lambda}_1}\right|_{\bar{\lambda}_1=\bar{\lambda}_2=\bar{\lambda}_3=1} = \left.\frac{\partial P_1^{\mathrm{D}}}{\partial \bar{\lambda}_3 \partial \bar{\lambda}_1}\right|_{\bar{\lambda}_1=\bar{\lambda}_2=\bar{\lambda}_3=1} = \begin{cases} \dfrac{-2+14w^2+3w^4}{2(-1+w^2)^3} + \dfrac{15w^3\arccos(w)}{2(1-w^2)^{7/2}} & w<1 \\ 3/7 & w=1 \\ \dfrac{-2+14w^2+3w^4}{2(-1+w^2)^3} - \dfrac{15w^3\operatorname{arccosh}(w)}{2(-1+w^2)^{7/2}} & w>1 \end{cases},$$

$$\left.\frac{\partial P_1^{\mathrm{D}}}{\partial \bar{\lambda}_3 \partial \bar{\lambda}_2}\right|_{\bar{\lambda}_1=\bar{\lambda}_2=\bar{\lambda}_3=1} = \begin{cases} \dfrac{-8w^2-9w^4+2w^6}{8(-1+w^2)^3} - \dfrac{15w^3\arccos(w)}{8(1-w^2)^{7/2}} & w<1 \\ 1/7 & w=1 \\ \dfrac{-8w^2-9w^4+2w^6}{8(-1+w^2)^3} + \dfrac{15w^3\operatorname{arccosh}(w)}{8(-1+w^2)^{7/2}} & w>1 \end{cases}.$$

References

Bednarek, S., 1999. The giant magnetostriction in ferromagnetic composites within an elastomer matrix. Appl. Phys. A. Mater. Sci. Process. 68, 63–67.

Borcea, L., Bruno, O., 2001. On the magneto-elastic properties of elastomer-ferromagnet composites. J. Mech. Phys. Solids 49, 2877–2919.

Coleman, B.D., Noll, W., 1963. The thermodynamics of elastic materials with heat conduction and viscosity. Arch. Ration. Mech. Anal. 13, 167–178.
Diguet, G., Beaugnon, E., Cavaille, J.Y., 2010. Shape effect in the magnetostriction of ferromagnetic composite. J. Magn. Magn. Mater. 322, 3337–3341.
Duenas, T., Carman, G., 2000. Large magnetostrictive response of Terfenol-D resin composites (invited). J. Appl. Phys. 87, 4696–4701.
Galipeau, E., 2012. Homogenization of Magnetorheological Elastomers. Ph.D. Thesis. The University of Pennsylvania.
Galipeau, E., Ponte Castañeda, P., in preparation. A two dimensional constitutive model for magnetorheological elastomers at finite strains and rotations.
Ginder, J., Clark, S., Schlotter, W., Nichols, M., 2002. Magnetostrictive phenomena in magnetorheological elastomers. Int. J. Mod. Phys. B 16, 2412–2418.
Guan, X., Dong, X., Ou, J., 2008. Magnetostrictive effect of magnetorheological elastomer. J. Magn. Magn. Mater. 320, 158–163.
Jolly, M., Carlson, J., Munoz, B., 1996. A model of the behaviour of magnetorheological materials. Smart Mater. Struct. 5, 607–614.
Kankanala, S., Triantafyllidis, N., 2004. On finitely strained magnetorheological elastomers. J. Mech. Phys. Solids 52, 2869–2908.
Kaye and Laby Tables of Physical and Chemical Constants. 2011. Magnetic properties of materials. <http://www.kayelaby.npl.co.uk/general_physics/2_6/2_6_6.html>.
Kovetz, A., 2000. Electromagnetic Theory. Oxford University Press.
Lanotte, L., Ausanio, G., Iannotti, V., Luponio, C., 2003. Influence of particle pre-orientation on elastomagnetic effect in a composite material of ellipsoidal Ni microparticles in a silicone matrix. Appl. Phys. A. Mater. Sci. Process. 77, 953–958.
Liu, L., James, R., Leo, P., 2006. Magnetostrictive composites in the dilute limit. J. Mech. Phys. Solids 54, 951–974.
Pelrine, R., Kornbluh, R., Joseph, J., Heydt, R., Pei, Q., Chiba, S., 2000. High-field deformation of elastomeric dielectrics for actuators. Mater. Sci. Eng. C 11, 89–100.
Ponte Castañeda, P., 1992. Bounds and estimates for the properties of nonlinear heterogeneous systems. Philos. Trans. R. Soc. B 340, 531–567.
Ponte Castañeda, P., 1998. Three-point bounds and other estimates for strongly nonlinear composites. Phys. Rev. B 57, 12077–12083.
Ponte Castañeda, P., Galipeau, E., 2011. Homogenization-based constitutive models for magnetotheological elastomers at finite strain. J. Mech. Phys. Solids 59, 194–215.
Ponte Castañeda, P., Siboni, M.H., 2011. A finite-strain constitutive theory for electro-active polymer composites via homogenization. Int. J. Nonlinear Mech., in press. doi:10.1016/j.ijnonlinmec.2011.06.012.
Ponte Castañeda, P., Willis, J., 1995. The effect of spatial-distribution on the effective behavior of composite-materials and cracked media. J. Mech. Phys. Solids 43, 1919–1951.
Siboni, M.H., Ponte Castañeda, P., 2011a. The response of an ellipsoidal, magnetically anisotropic inclusion in a linear elastic medium to a nonaligned magnetic field. Comptes Rendus Mécanique.
Siboni, M.H., Ponte Castañeda, P., 2011b. Magnetorheological elastomers: dilute estimates, in preparation.
Willis, J., 1977. Bounds and self-consistent estimates for overall properties of anisotropic composites. J. Mech. Phys. Solids 25, 185–202.
Yin, H., Sun, L., Chen, J., 2006. Magneto-elastic modeling of composites containing chain-structured magnetostrictive particles. J. Mech. Phys. Solids 54, 975–1003.
Yin, H.M., Sun, L.Z., 2006. Magnetoelastic modelling of composites containing randomly dispersed ferromagnetic particles. Philos. Mag. 86, 4367–4395.